Soft Matter

# Relaxation dynamics of deformed polymer nanocomposites as revealed by small-angle scattering and rheology



| | |
|---|---|
| Journal: | *Soft Matter* |
| Manuscript ID | SM-ART-06-2022-000775.R2 |
| Article Type: | Paper |
| Date Submitted by the Author: | 17-Oct-2022 |
| Complete List of Authors: | Sun, Ruikun; Michigan State University<br>Yang, Jie; Michigan State University; Sichuan University<br>Patil, Shalin; Michigan State University<br>Liu, Yun; National Institute of Standards and Technology; University of Delaware<br>Zuo, Xiaobing; Argonne National Laboratory,<br>Lee, Andre; Michigan State University, Chemical Engineering and Materials Science<br>Yang, Wei; Sichuan University, College of Polymer Science and Engineering<br>Wang, Yangyang; Oak Ridge National Laboratory, Center for Nanophase Materials Sciences<br>Cheng, Shiwang; Maurice Morton Institute of Polymer Science and Engineering, Department of Chemical Engineering and Materials Science |
| | |

# Relaxation dynamics of deformed polymer nanocomposites as revealed by small-angle scattering and rheology

Ruikun Sun,[1] Jie Yang,[1,2] Shalin Patil,[1] Yun Liu,[3,4] Xiaobing Zuo,[5] Andre Lee,[1] Wei Yang,[2] Yangyang Wang,[6*] and Shiwang Cheng[1†]

[1]*Department of Chemical Engineering and Materials Science, Michigan State University, East Lansing, MI 48824, United States*
[2]*College of Polymer Science and Engineering, State Key Laboratory of Polymer Materials Engineering, Sichuan University, Chengdu, Sichuan 610065, People's Republic of China*
[3]*Center for Neutron Research, National Institute of Standards and Technology, Gaithersburg, Maryland 20899, United States*
[4]*Department of Chemical and Biomolecular Engineering, University of Delaware, Newark, Delaware 19716, United States*
[5]*X-ray Science Division, Argonne National Laboratory, Lemont, Illinois 60439, United States*
[6]*Center for Nanophase Materials Sciences, Oak Ridge National Laboratory, Oak Ridge, Tennessee 37831, United States*

## Abstract

The relaxation dynamics of polystyrene (PS)/silica nanocomposites after a large step deformation are studied by a combination of small-angle scattering techniques and rheology. Small-angle x-ray scattering measurements and rheology show clear signatures of nanoparticle aggregation that enhances the mechanical properties of the polymer nanocomposites (PNCs) in the linear viscoelastic regime and during the initial phase of stress relaxation along with accelerated relaxation dynamics. Small-angle neutron scattering experiments under the zero-average-contrast condition reveal, however, smaller structural anisotropy in the PNCs than that in the neat polymer matrix, as well as accelerated anisotropy relaxation. In addition, the degrees of anisotropy reduction and relaxation dynamics acceleration increase with increasing nanoparticle loading. These results are in sharp contrast to the prevailing viewpoint of enhanced molecular deformation as the main mechanism for the mechanical enhancement in PNCs. Furthermore, the observed acceleration of stress relaxation and reduction in structural anisotropy point to two types of nonlinear effects in the relaxation dynamics of PNCs at large deformation.

* † Corresponding Authors. Email Addresses: wangy@ornl.gov, chengsh9@msu.edu

## Introduction

Mechanical reinforcement in polymer nanocomposites (PNCs) has a complex origin. An important mechanism of reinforcement in PNCs is the so-called hydrodynamic effect[1-11], which has been extensively studied both theoretically and experimentally. In the case of dilute suspensions (volume fraction of particulates smaller than ~2-3%, assuming no aggregations)[12], analyses with the hydrodynamic equations[1-5, 7, 13-16] indicate that the presence of solid particles distorts the velocity or displacement fields of the surrounding medium, and at the same time gives rise to an enhancement in viscosity or modulus. However, such analyses become increasingly difficult at higher particle concentrations[17], and the reinforcement mechanism in PNCs with high nanoparticle (NP) loadings remains an area of active research[18-31]. To explain the high mechanical strength of filled rubbers at large deformation, Mullins and Tobin[6] introduced the concept of strain amplification, arguing that the presence of non-deformable fillers produces enhanced microscopic deformation in the polymer matrix[32]. While this concept of strain amplification has been widely used in the polymer community[33, 34], it has also led to considerable confusion. In particular, there have been conflicting experimental reports on microscopic evidence of molecular overstraining[35-38]. Recently, our combined rheology and small-angle neutron scattering (SANS) experiments[39] on poly(methyl methacrylate) (PMMA) and silica ($SiO_2$) nanocomposites revealed that the average structural anisotropy of the polymer matrix was not amplified by NPs, due to a redistribution of strain field akin to the classical hydrodynamic picture of Einstein and Smallwood[1]. This finding offers a key clue to understanding the microscopic reinforcement mechanism in polymer nanocomposites.

This work further exploits the relaxation dynamics in a series of nanocomposites of polystyrene (PS) and silica nanoparticles after a step uniaxial extension. The current investigation

differs from the previous study[39] in multiple ways. First, in addition to SANS, small-angle x-ray scattering (SAXS) is employed to monitor the spatial distribution of nanoparticles in both the undeformed and deformed states. The combination of SANS and SAXS provides complementary structural information on the polymer matrix and nanoparticles. Secondly, compared with the PMMA/$SiO_2$ system, the dispersion of silica nanoparticles in polystyrene is poor due to the non-attractive polymer-nanoparticle interactions, leading to the formation of NP clusters and networks. Lastly, compared with a moderate loading of 8 v% in the previous work, significantly higher NP concentrations up to 24 v% are surveyed in the current study.

The results of the current investigation are in broad agreement with the prior findings from the PMMA/$SiO_2$ system, lending further support to the hydrodynamic reinforcement mechanism of PNCs[39]. In addition, new intriguing phenomena have been revealed, including the reduced polymer structural anisotropy and accelerated relaxation dynamics, in PS/$SiO_2$ nanocomposites with considerable NP aggregates and networks, pointing to two types of previously not well-discussed nonlinear effects associated with the redistribution of strain field in the vicinity of nanoparticles.

## Experimental

### Materials

Protonated polystyrene ($H^8$-PS) with weight average molecular weight ($M_w$) of $310\ kg/mol$ and polydispersity index (PDI) of $1.05$ was purchased from Scientific Polymer Products, Inc. Deuterated polystyrene ($D^8$-PS, degree of Deuteration > 97%) with $M_w = 304\ kg/mol$ was obtained from Polymer Source, Inc. Both were used as received. Suspensions of bare spherical silica ($SiO_2$) nanoparticles (TEM images see Ref. 27 and Ref. 40) with average radius $R = 7 \pm 2$ nm (polydispersity of $pd \approx 0.30$) in methyl ethyl ketone (MEK) were supplied by the Nissan

Chemical America Corporation. To remove the surfactants in the original NP suspensions, a solvent exchange procedure was applied to the silica/MEK suspension to replace MEK with tetrahydrofuran (THF). Specifically, NPs in the silica/MEK suspension were precipitated in hexane and redispersed in tetrahydrofuran (THF) to a concentration of 40 mg/mL. The NPs after the solvent exchange were used in the preparation of all PNCs. PS/$SiO_2$ nanocomposites were prepared by a solution casting method following a previous protocol[40-42]. First, $H^8$-PS and $D^8$-PS of desired ratios were dissolved in THF to a concentration of $0.005\ \mathrm{g/mL}$. A trace amount of Irganox® 1010 antioxidant (0.01 wt% with respect to the mass of the polymer) was added to the solution at this stage. This parent solution was then passed through a poly(tetrafluoroethylene) (PTFE) filter with the pore size of $20\ \mu\mathrm{m}$ to remove impurities and dusts. The filtered PS/THF solution was transferred to glass flasks, where different amounts of $SiO_2$/THF suspension were added to achieve the desired nanoparticle loadings. The PS/$SiO_2$/THF mixtures were dried in a rotary evaporator, forming a thin film on the inner surface of the flask. The PS/$SiO_2$ film was removed from the flask and dried at $413\ \mathrm{K}$ under vacuum ($10^{-2}$ torr (~1.33 Pa)) for 48 hours before further characterization. Two sets of PS/$SiO_2$ nanocomposites were prepared. The first set of PS/$SiO_2$ was prepared for the sole purpose of identifying the zero-average-contrast (ZAC) condition for SANS. The loading of nanoparticles was fixed at 8 v% and the ratio of the hydrogenous PS to deuterated PS (H/D ratio) varied from 0.35:0.65 to 0.90:0.10. The second set of PS/$SiO_2$ was made for the combined small-angle scattering and rheology study, which was the focus of this work. The H/D ratio of PS was fixed at the contrast matching point, 0.57:0.43, while the volume fraction of $SiO_2$ varied from 8.7 v% to 18 v% to 24 v%. Note that the 8.7 v% with H/D = 0.57:0.43 was also used for the ZAC point identification. The compositions of these two sets of PS/$SiO_2$ nanocomposites are summarized in **Table 1**.

**Table 1** Compositions of PS/$SiO_2$ nanocomposites

| Sample name | | $SiO_2$ loading (v%) | H/D ratio |
|---|---|---|---|
| Zero average contrast identification | CM1 | 8 | 0.35:0.65 |
| | CM2 | 8 | 0.50:0.50 |
| | CM3 | 8 | 0.55:0.45 |
| | CM4 | 8 | 0.60:0.40 |
| | CM5 | 8 | 0.65:0.35 |
| | CM6 | 8 | 0.80:0.20 |
| | CM7 | 8 | 0.90:0.10 |
| Structural anisotropy quantification | PS0 | 0 | 0.57:0.43 |
| | PS8.7 | 8.7 | 0.57:0.43 |
| | PS18 | 18 | 0.57:0.43 |
| | PS24 | 24 | 0.57:0.43 |

**Thermogravimetric analysis (TGA)**

TGA analysis (Q50, TA Instruments) was employed to identify the mass fraction $m_{\mathrm{NP}}$ of the nanoparticles in the PNCs. The samples were heated in an air atmosphere from 313 K to 1073 K with a constant rate of 20 K/min. The volume fraction of the NPs, $\phi_{\mathrm{NP}}$, was obtained through the relation $\phi_{\mathrm{NP}} = \frac{m_{\mathrm{NP}}/\rho_{\mathrm{NP}}}{m_{\mathrm{NP}}/\rho_{\mathrm{NP}} + (1-m_{\mathrm{NP}})/\rho_{\mathrm{p}}}$ with $\rho_{\mathrm{NP}} = 2.16\ \mathrm{g/cm^3}$ and $\rho_{\mathrm{p}} = 1.05\ \mathrm{g/cm^3}$ being the mass densities of the nanoparticle[43] and polymer, respectively.

**Rheology**

Small-amplitude oscillatory shear (SAOS) experiments were conducted on an Anton Paar MCR302 rheometer with a pair of parallel plates of 8 mm in diameter. Prior to loading, the PNC samples were molded into disks of 8 mm in diameter and 1 mm in thickness by a hydraulic press (Carver, Inc.) at 453 K, which is more than 1.2 times of the glass transition temperature, $T_g$, of PNCs[44]. The frequency sweep measurements in the range of $10^2$-$10^{-2}$ rad/s were performed

between 383 K and 453 K with an interval of 10 K. The gap was adjusted accordingly during the measurements at different temperatures to ensure accurate measurements of modulus. The applied strain amplitude was in the linear response region varying from 0.1% to 1% depending on the testing temperature and NP loadings. Linear viscoelastic master curves of the PNCs were constructed through the time-temperature superposition principle[45].

Stress relaxation experiments of the neat matrix polymer and PNCs were carried out on an RSA-III solid analyzer (TA Instruments) at $T = 393$ K and $T = 400$ K. The samples were uniaxially stretched to an elongation ratio $\lambda = 1.8$ with a constant Hencky strain rate of $\dot{\varepsilon} = 0.01$ $\mathrm{s}^{-1}$ at $T = 393$ K, and to $\lambda = 1.2$ and $1.5$ with $\dot{\varepsilon} = 0.1\ \mathrm{s}^{-1}$ at $T = 400$ K. The Weissenberg numbers $\dot{\varepsilon}\tau$ were approximately the same for the step deformations at 393 K and 400 K, where the $\tau$ is the terminal relaxation time of the neat polymer defined by the low-frequency crossover of the storage and loss moduli. These deformation rates fall in the middle of the rubbery plateau region and thus should not invoke any glassy response. The experiments at $\lambda = 1.2$, and 1.5 at $T = 400$ K were performed to examine the stress relaxation behavior of PNCs; the samples during stress relaxation at $\lambda = 1.8$ at $T = 393\,K$ were measured by small-angle scattering techniques. Specifically, the stress relaxation at $\lambda = 1.8$ was terminated at $t = 0\ \tau$, $0.01\ \tau$, $0.03\ \tau$, $0.1\ \tau$, $0.3\ \tau$, and $1.0\ \tau$ (with $\tau = 3.958 \times 10^4$ s being the terminal relaxation time of the neat polymer at $T = 393\ K$) by rapidly quenching the sample below the glass temperature. We chose $T = 393$ K as the test temperature so that the effective quenching time (less than ~10 s) was significantly shorter than the terminal relaxation time of the polymer matrix. The structures of the undeformed and deformed PS and PS/$SiO_2$ nanocomposites were investigated by small-angle scattering techniques (SAXS and SANS).

### Small-angle x-ray scattering (SAXS)

SAXS measurements were conducted at the 12-ID-B beamline of the Advanced Photon Source at the Argonne National Laboratory. The energy of the incident x-ray beam was 13.3 keV ($\lambda = 0.935$ Å). In all measurements, the sample-to-detector distance was 2 m and a two-dimensional (2D) Pilatus 2M detector was used. The scattering angles were calibrated with silver behenate and the absolute scattering intensity was determined from a glassy carbon standard.

### Small-angle neutron scattering (SANS)

SANS measurements were performed on the NGB30 SANS beamline at the Center for Neutron Research (NCNR) of the National Institute of Standards and Technology (NIST). Three different configurations were used to cover a wide range of scattering wavenumbers of $0.004 - 0.3$ Å$^{-1}$. The measured scattering intensity was corrected for the detector background and sensitivity, and placed on an absolute scale using direct beam measurements. Using the values of Kuhn length $l_{\mathrm{K}}$ and radius of gyration $R_{\mathrm{G}}$ from the literature[46, 47], we find that $\pi/l_{\mathrm{K}} \approx 0.19$ Å$^{-1}$ and $\pi/R_{\mathrm{G}} \approx 0.02$ Å$^{-1}$ that are well covered by the instrument.

## Technical background

### Zero-average-contrast (ZAC) approach to polymer nanocomposites

For mixtures of hydrogenous and deuterated polymers of matching chain lengths, the measured coherent scattering intensity is proportional to the single-chain structure factor (also called the form factor of a polymer chain)[48-51]. However, the determination of single-chain conformation in polymer nanocomposites is strongly hampered by the presence of nanoparticles[35, 52-54]. Fortunately, such a problem can be resolved or at least minimized by adopting a zero-average-contrast approach[55-60].

For a polymer nanocomposite containing nanoparticles, and hydrogenous and deuterated polymers of matching molecular weights, the (volume normalized) coherent scattering intensity $I(\mathbf{Q})$ is given by[55]

$$I(\mathbf{Q}) = (\rho_{\mathrm{H}} - \rho_{\mathrm{D}})^2 \phi(1-\phi) \frac{\phi_{\mathrm{p}}}{\nu_{\mathrm{chain}}} S_{\mathrm{intra}}(\mathbf{Q}) + [\phi\rho_{\mathrm{H}} + (1-\phi)\rho_{\mathrm{D}} - \rho_0]^2 \left[ \frac{\phi_{\mathrm{p}}}{\nu_{\mathrm{chain}}} S_{\mathrm{intra}}(\mathbf{Q}) + V_{\mathrm{p}} \phi_{\mathrm{p}} S_{\mathrm{inter}}(\mathbf{Q}) \right], \quad (1)$$

where $\mathbf{Q}$ is the scattering wave vector, $\rho_{\mathrm{H}}$, $\rho_{\mathrm{D}}$, and $\rho_0$ are respectively the scattering length densities (SLDs) of the hydrogenous polymers, deuterated polymers, and NPs, $\phi$ is the volume fraction of the hydrogenous chains in polymer phase, $\phi_{\mathrm{p}}$ is the volume fraction of polymer phase in the PNC, $V_{\mathrm{p}}$ is the total volume of polymer phase, and $\nu_{\mathrm{chain}}$ is the number density of chains in the polymer phase. The normalized intrachain [$S_{\mathrm{intra}}(\mathbf{Q})$] and interchain [$S_{\mathrm{inter}}(\mathbf{Q})$] partial structure factors defined as follows:

$$S_{\mathrm{intra}}(\mathbf{Q}) \equiv \frac{1}{MN^2} \sum_{\alpha}^{M} \sum_{m,n}^{N} \left\langle e^{-i\mathbf{Q} \cdot (\mathbf{R}_{\alpha,m} - \mathbf{R}_{\alpha,n})} \right\rangle, \quad (2)$$

$$S_{\mathrm{inter}}(\mathbf{Q}) \equiv \frac{1}{M(M-1)N^2} \sum_{\alpha \neq \beta}^{M} \sum_{m,n}^{N} \left\langle e^{-i\mathbf{Q} \cdot (\mathbf{R}_{\alpha,m} - \mathbf{R}_{\beta,n})} \right\rangle \approx \frac{1}{M^2N^2} \sum_{\alpha \neq \beta}^{M} \sum_{m,n}^{N} \left\langle e^{-i\mathbf{Q} \cdot (\mathbf{R}_{\alpha,m} - \mathbf{R}_{\beta,n})} \right\rangle. \quad (3)$$

where $M$ is the total number of chains, $N$ is the chain length (number of segments per chain), and $\mathbf{R}_{\alpha,m}$ is the position vector of segment $m$ in chain $\alpha$. When the average contrast $\phi\rho_{\mathrm{H}} + (1-\phi)\rho_{\mathrm{D}} - \rho_0$ is zero, Eq. (1) becomes:

$$I(\mathbf{Q}) = (\rho_{\mathrm{H}} - \rho_{\mathrm{D}})^2 \phi(1-\phi) \frac{\phi_{\mathrm{p}}}{\nu_{\mathrm{chain}}} S(\mathbf{Q}), \quad (4)$$

with $S(\mathbf{Q}) \equiv S_{\text{intra}}(\mathbf{Q})$. In other words, by matching the average SLD of the hydrogenous and deuterated polymers to the SLD of the nanoparticle, the single-chain structure factor of the polymer matrix can be obtained by SANS. A detailed derivation and additional comments of Eq. (4) is given in the Appendix.

**Spherical harmonic expansion analysis of deformed polymers**

To quantify the nonequilibrium structures of PNCs as well as the pristine polymer, the spherical harmonic expansion (SHE) technique[39, 51, 61-67] is employed in the analysis of the 2D SANS and SAXS spectra. As explained in the preceding discussion, the ZAC approach allows us to access the single-chain structure factor $S(\mathbf{Q})$ of the polymer matrix in PNCs. Specifically, the $S($ $\mathbf{Q})$ can be calculated from the following formula:

$$S(\mathbf{Q}) = \frac{I_{\text{coh}}(\mathbf{Q})}{\phi_{\text{p}} \lim_{Q\to 0} I_{\text{iso,neat}}(Q)} \approx \frac{I(\mathbf{Q})}{\phi_{\text{p}} \lim_{Q\to 0} I_{\text{iso,neat}}(Q)}, \tag{5}$$

where $I_{\text{coh}}(\mathbf{Q})$ is the coherent scattering intensity, and $\lim_{Q\to 0} I_{\text{iso,neat}}(Q)$ is the zero-angle scattering intensity of the pristine polymer melt in the isotropic state. Strictly speaking, the incoherent scattering "background" $I_{\text{inc}}$ should be subtracted from the total scattering intensity $I(\mathbf{Q})$ to produce the "correct" single-chain structure factor[51]. However, this subtraction procedure is not carried in our current analysis, due to three reasons. First, the coherent scattering from the PNC dominates the signal at low $Q$, which is the region we are most interested in. Secondly, since the incoherent background is isotropic, it will not contribute to the anisotropic components of the spherical harmonic expansion. Lastly, $I_{\text{inc}}$ can *only* be estimated from a model-dependent fitting procedure[51]. In the case of uniaxial extension, the single-chain structure factor can be expanded by spherical harmonics as[65]:

$$S(\mathbf{Q}) = \sum\nolimits_{l:\text{even}} S_l^0(Q) Y_l^0(\theta,\varphi) = \sum\nolimits_{l:\text{even}} S_l^0(Q)\sqrt{2l+1} P_l^0(\cos\theta). \tag{6}$$

Here, the stretching is along the $z$-axis of the spherical coordinates. $\theta$ is the polar angle and $\varphi$ is the azimuthal angle. $Y_l^0(\theta,\varphi)$ and $P_l^0(x)$ are respectively the spherical harmonics and associated Legendre functions of degree $l$ and order 0. $S_l^0(Q)$ is the $Q$-dependent spherical harmonic expansion coefficient, and can be evaluated from the measured 2D SANS spectra as:

$$\begin{aligned} S_l^0(Q) &= \frac{1}{2}\int_0^\pi S(Q,\theta,\varphi=0)\sqrt{2l+1} P_l^0(\cos\theta)\sin\theta \mathrm{d}\theta \\ &= \frac{1}{2\phi_\mathrm{p}\lim\limits_{Q\to 0} I_\mathrm{iso,neat}(Q)}\int_0^\pi I_{xz}(Q,\theta)\sqrt{2l+1} P_l^0(\cos\theta)\sin\theta \mathrm{d}\theta, \end{aligned} \tag{7}$$

where $I_{xz}(Q,\theta)$ is the scattering intensity associated with the 2D SANS spectrum. $S_0^0(Q)$ is the isotropic expansion coefficient, whereas $S_l^0(Q)$ ($l \geq 2$) are the anisotropic expansion coefficients. Further details of the spherical harmonic expansion technique can be found in our previous work[39, 51, 64-67]. It is worth noting that the orthogonality and normalization relation for our spherical harmonic functions is:

$$\int_0^{2\pi} \mathrm{d}\varphi \int_0^\pi \sin\theta \mathrm{d}\theta Y_l^m(\theta,\varphi) Y_{l'}^{m'}(\theta,\varphi) = 4\pi\delta_{ll'}\delta_{mm'}, \tag{8}$$

where $\delta_{ll'}$ and $\delta_{mm'}$ are Kronecker delta functions. Additionally, the associated Legendre functions in our work[65] include the Condon-Shortly phase factor $(-1)^m$. Because of the symmetry requirements[64, 65], $m$ is always even and this detail has no practical importance. Lastly, the leading anisotropic expansion coefficient $S_2^0(Q)$ has a close connection to the entropic stress[39, 67, 68].

Similarly, the spherical harmonic expansion analysis can be applied to the 2D SAXS spectra of the PNCs. Due to the high polydispersity of the silica nanoparticles ($pd \approx 0.30$), we are unable to obtain direct information on the spatial distribution of NPs (interparticle structure factor) by

simply dividing the scattering intensity by a "form factor"[69-71]. Nevertheless, the scattering intensity $I(\mathbf{Q})$ can be expanded by spherical harmonics as:

$$I(\mathbf{Q}) = \sum_{l:\text{even}} I_l^0(Q) Y_l^0(\theta,\varphi) = \sum_{l:\text{even}} I_l^0(Q)\sqrt{2l+1} P_l^0(\cos\theta). \quad (9)$$

The corresponding spherical harmonic expansion coefficients $I_l^0(Q)$ can be obtained by the integral:

$$I_l^0(Q) = \frac{1}{2}\int_0^\pi I_{xz}(Q,\theta)\sqrt{2l+1} P_l^0(\cos\theta)\sin\theta \mathrm{d}\theta, \quad (10)$$

where $I_{xz}(Q,\theta)$ is the scattering intensity given by the 2D SAXS detector. To evaluate Eq. (10) from the experimental data, the scattering intensities $I(Q_x,Q_z)$ in the Cartesian coordinates are first tabulated in the terms of the polar coordinates. $I_{xz}(Q,\theta_i)$ belong to the same bin of $Q$ are used to calculate $I_l^0(Q)$: $I_l^0(Q) = \frac{\pi}{2N}\sum_{i=1}^{N} I_{xz}(Q,\theta_i)\sqrt{2l+1} P_l^0(\cos\theta_i)\sin\theta_i$. Because of the symmetry of uniaxial extension, it suffices to compute $\sin\theta_i$ and $\cos\theta_i$ as: $\sin\theta_i = |Q_x|/\sqrt{Q_x^2+Q_z^2}$ and $\cos\theta_i = |Q_z|/\sqrt{Q_x^2+Q_z^2}$.

The details and benefits of the spherical harmonic expansion analysis have been discussed in our previous publications[39, 64-67, 72]. We note that the traditional methods of analyzing the scattering intensities in the parallel and perpendicular directions[35, 37] yield only partial structural information[39, 51]. Moreover, analysis of the gyration tensor often faces practical challenges[65] and can provide only a coarse-grained picture of molecular deformation. By contrast, the spherical harmonic expansion approach circumvents the problems in polymer radius of gyration analysis and makes full use of the structural information in 2D small-angle scattering spectra.

# Results

## Rheology of PNCs

**Figure 1(a)** presents the linear viscoelastic master curves of the PNCs as well as the neat matrix polymer at a reference temperature $T = 393\ K$, where the storage $[G'(\omega)]$ and loss $[G''(\omega)]$ moduli are shown as a function of the angular frequency $\omega$, along with the dynamic shift factors $a_T$. The shift factor can be described by the Williams-Landel-Ferry equation $\log a_T = -\frac{C_1(T-T_0)}{C_2+T-T_0}$, where $C_1 = 9.03 \pm 0.5$, $C_2 = 60 \pm 3$ K, and the reference temperature $T_0 = 393$ K, consistent with the result of a previous publication[73]. No vertical shifts are needed for the construction of master curves. Although the master curves construction of PNCs remains a topic of active debate[40], the elastic moduli of PNCs in the rubbery plateau region is typically not strongly influenced by the choice of construction protocol. Two key features are worth noting. First, the rubbery plateau moduli of PNCs are significantly higher than that of the neat matrix polymer. Second, no terminal relaxation region is observed for the PNCs within the experimental frequency range and a second plateau region can be resolved at low frequencies. In other words, strong mechanical reinforcement is found in PNCs over a wide frequency range. Furthermore, the loss factors $\tan\delta \equiv G''/G'$ [**Figure 1(b)**] of all samples are almost identical at intermediate and high frequencies, suggesting that the mechanical reinforcement in the rubbery plateau region is primarily hydrodynamic in nature. We note that polymer bridges in principle can contribute to the mechanical properties of PNCs[27, 40, 74, 75]. However, only polymer bridges shorter than the entanglement molecular weight can give enhancement to the plateau modulus of PNCs. Since the PNCs and neat PS exhibit almost identical loss tangents in the high frequency, Rouse region (Figures 1a and 1b), the amount of short bridges should be small in the current system that plays a secondary role in mechanical reinforcement in the rubbery plateau region. The concentration ($\phi_{SiO_2}$) dependence of plateau

modulus $G_{\mathrm{pl}}(\phi_{\mathrm{SiO_2}})$ is shown in **Figure 2(a)**, along with the predictions of the Einstein-Smallwood[1, 3], $G_{\mathrm{pl}}(\phi_{\mathrm{SiO_2}})/G_{\mathrm{pl}}(0) = 1 + 2.5\phi_{\mathrm{SiO_2}}$, and Guth-Gold[2], $G_{\mathrm{pl}}(\phi_{\mathrm{SiO_2}})/G_{\mathrm{pl}}(0) = 1 + 2.5\,\phi_{\mathrm{SiO_2}} + 14.1\phi_{\mathrm{SiO_2}}^2$, equations. Here, the plateau modulus is defined as the storage modulus at the frequency where the loss factor $\tan\delta$ displays a minimum and $\phi_{\mathrm{SiO_2}}$ is the volume fraction of nanoparticles. The stronger reinforcement effect relative to the Einstein-Smallwood and the Guth-Gold relations is commonly seen in PNCs, which has been attributed to a higher *effective pervaded volume* of NPs and the presence of NP clusters[10, 25, 76]. On the other hand, the emergence of low-frequency plateau is often attributed to the NP network or polymer bridge network[27, 40]. The formation of NP network in PNCs is also consistent with the non-dissolvable nature of these PNCs in good solvent, such as THF. Aggregation of $SiO_2$ nanoparticles in PS is not surprising and may be attributed to the repulsive PS-$SiO_2$ interaction. As we shall show below, the SAXS measurements also support the existence of large particle aggregates in the PS/$SiO_2$ nanocomposites. We emphasize that the current study focuses on the relaxation dynamics of PNCs at intermediate time scales, where hydrodynamic reinforcement dominates.

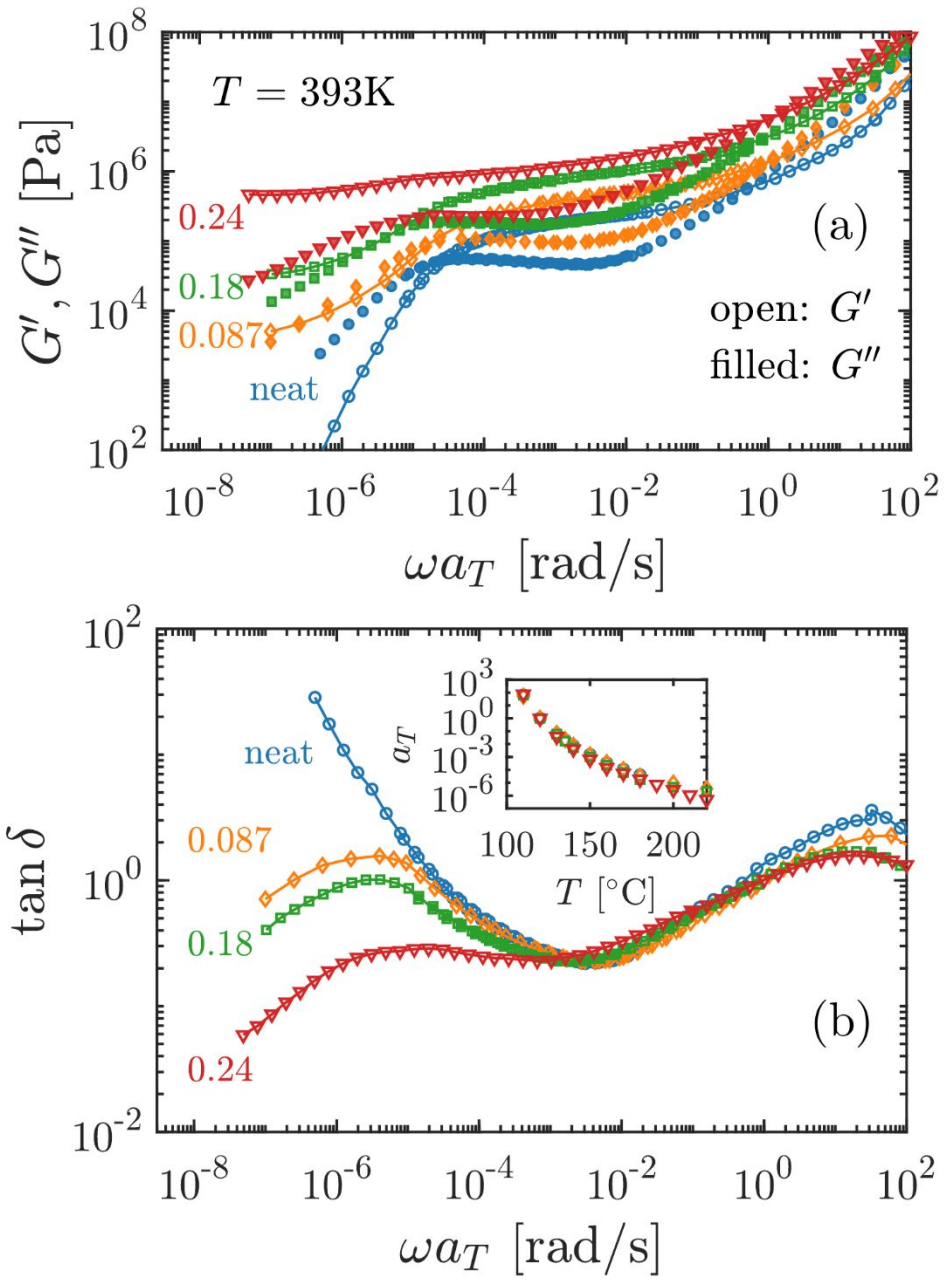


**Figure 1.** (a) Linear viscoelastic spectra of neat PS and PNCs at 393 K. Open symbols: $G'$. Filled symbols: $G''$. $a_T$ is the shift factor. (b) Corresponding loss factor $tan\,\delta \equiv G''/G'$. Inset: dynamic shift factors.

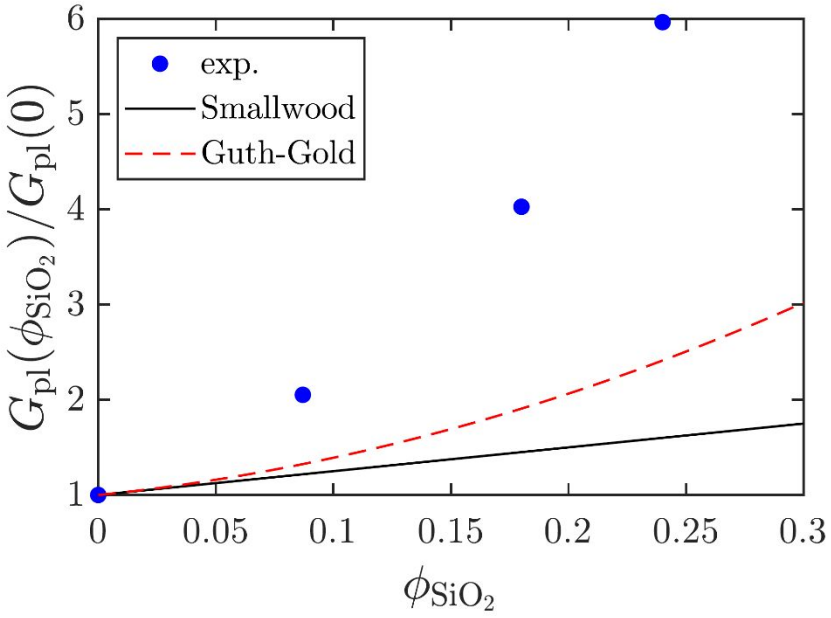


**Figure 2.** Dependence of the rubbery plateau modulus $G_{pl}$ on the volume fraction of silica nanoparticles $\phi_{SiO_2}$. Solid line: Einstein-Smallwood equation: $G_{pl}(\phi_{SiO_2})/G_{pl}(0) = 1 + 2.5\phi_{SiO_2}$. Dashed line: Guth-Gold equation: $G_{pl}(\phi_{SiO_2})/G_{pl}(0) = 1 + 2.5\phi_{SiO_2} + 14.1\phi_{SiO_2}^2$.

**Figure 3a-3c** show the evolution of engineering stress $\sigma(t) = F(t)/A_0$ of PNCs and the neat matrix polymer at $\lambda = 1.2$ (Hencky strain $\varepsilon \approx 0.18$), $\lambda = 1.5$ ($\varepsilon \approx 0.4$), and $\lambda = 1.8$ ($\varepsilon \approx 0.6$) and the subsequent stress relaxation, where $F(t)$ is the tensile force at time $t$ and $A_0$ is the initial cross-section area normal to the tensile force[77]. During deformation, all PNCs exhibit much higher stress than the neat polymer, and the degree of such enhancement increases with increasing nanoparticle loading. This behavior is in line with the linear viscoelastic properties of PNCs, where the rubbery plateau modulus $G_{\rm pl}$ grows rapidly with increasing nanoparticle volume fraction $\phi_{\rm SiO_2}$. Interestingly, the deformed neat polymer can retain the stress for a much longer time than the PNCs during stress relaxation, even at the smallest strain of $\lambda = 1.2$. This speedup in relaxation dynamics of deformed PNCs can be better illustrated by the normalized stress $\sigma(t_{\rm relax})/\sigma_0$ following the standard definition of stress relaxation[45], as shown in the inset of **Figure 3a-3c**. Here,

$\sigma_0$ is the engineering stress at the onset of stress relaxation and $t_{\text{relax}}$ the elapsed time during stress relaxation. Another important observation from **Figure 3a-3c** is that there are no signs of sudden losses of stress during stress during the initial relaxation or some long-lived relaxation modes for all PNCs up to 1 $\tau$ ($\tau = 3.958 \times 10^4$ s at T = 393 K) when the stress relaxation is almost complete.

The observation of accelerated stress relaxation in PNCs is intriguing. A "naïve" application of the Boltzmann superposition principle based on the linear viscoelastic data would predict a retarded relaxation in the PNCs, particularly for the ones with high nanoparticle loadings[45]. Nonlinear effects thus involve in the relaxation dynamics of PNCs at large deformation. **Figure 4a-4c** compare the stress relaxation of neat polymer and PNCs at different strains of $\lambda = 1.2, 1.5,$ and 1.8. For the neat PS (**Figure 4a**), the stress relaxation behavior does not change with the deformation up to $\lambda = 1.8$, consistent with previous measurements of stress relaxation of linear entangled polymers[65, 78]. Interestingly, both PS8.7 (**Figure 4b**) and PS24 (**Figure 4c**) show obvious strain dependence of the stress relaxation. The larger the deformation, the faster the stress relaxation. These observations are in agreement with the general expectation that incorporation of NPs can significantly reduce the linear response region of PNCs — nonlinear stress relaxation of PNCs can take place even at small strains.

External deformation can also lead to microstructure changes in PNCs, including breakup of NP agglomerates. However, a rigorous quantification of such structural rearrangements of PNCs with small-angle scattering techniques remains challenging: the methods developed in the previous studies of undeformed PNCs[79] cannot be applied directly to deformed PNCs with anisotropic structures. By contrast, the rheological behavior of PNCs is sensitive to the microstructure changes of NP agglomerates and can thus provide useful insights. **Figure 5** shows the stress ratios (reinforcement factors) of PNCs and the neat matrix polymer, $X = \sigma_{PNC}(\lambda)/\sigma_{neat}(\lambda)$, during the

step uniaxial extension, where the dashed lines represent the reinforcement factors predicted by the Guth-Gold relation. In each PNC, the stress ratio decreases gradually after the initial rise, approaching the hydrodynamic limit at large strains. Such a behavior is indicative of breakup of NP agglomerates. The breakup of NP agglomerates is consistent with the rather complete stress relaxation of PNCs in **Figure 3a**, further supporting the dominant polymer deformation for the high mechanical strength of PNCs. Despite the progressive reduction in the reinforcement factor, $X$ , with deformation, the experimental reinforcement factors at $\lambda = 1.8$ are *all* slightly higher than the hydrodynamic reinforcement factors of PNCs from the Guth-Gold relation, suggesting a slightly higher effective loading of NPs, $\phi_e$, in PNCs due to the residue NP aggregates. A rough estimate from the reinforcement factor shows $\phi_e - \phi_{SiO_2}$ is smaller than 10% for all the PNCs at $\lambda = 1.8$, and occluded polymers thus should not make any significant contributions to the stress relaxation and the structural anisotropy of deformed PNCs.

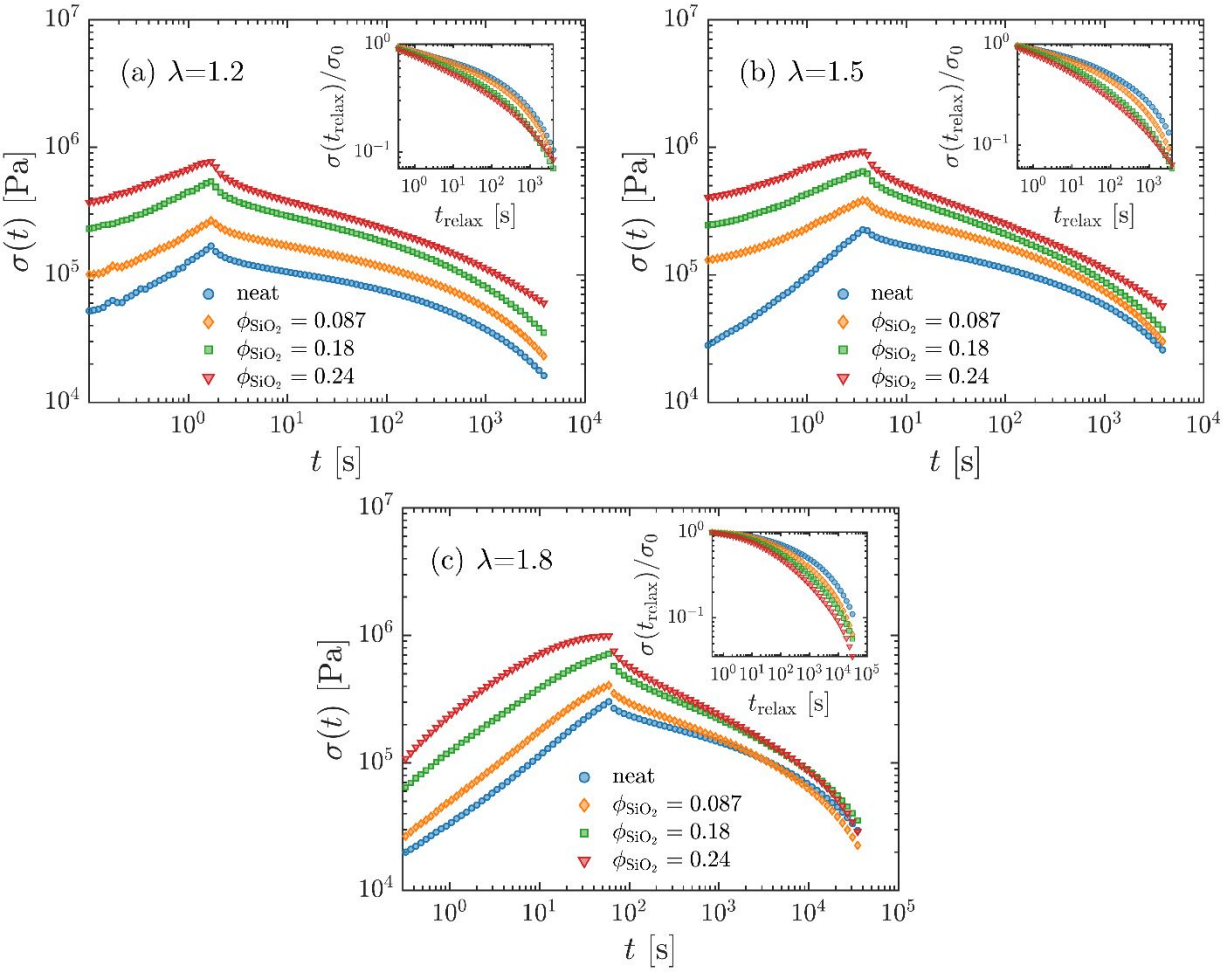


**Figure 3.** Evolution of engineering stress $\sigma(t)$ during stretching and stress relaxation for neat polymer and PNCs at (a) $\lambda = 1.2$ at $T = 400\,K$, (b) $\lambda = 1.5$ at $T = 400\,K$, and (c) $\lambda = 1.8$ at $T = 393\,K$. Inset: normalized stress $\sigma(t_{\text{relax}})/\sigma_0$ during stress relaxation, where $\sigma_0$ is the stress immediately after the step deformation.

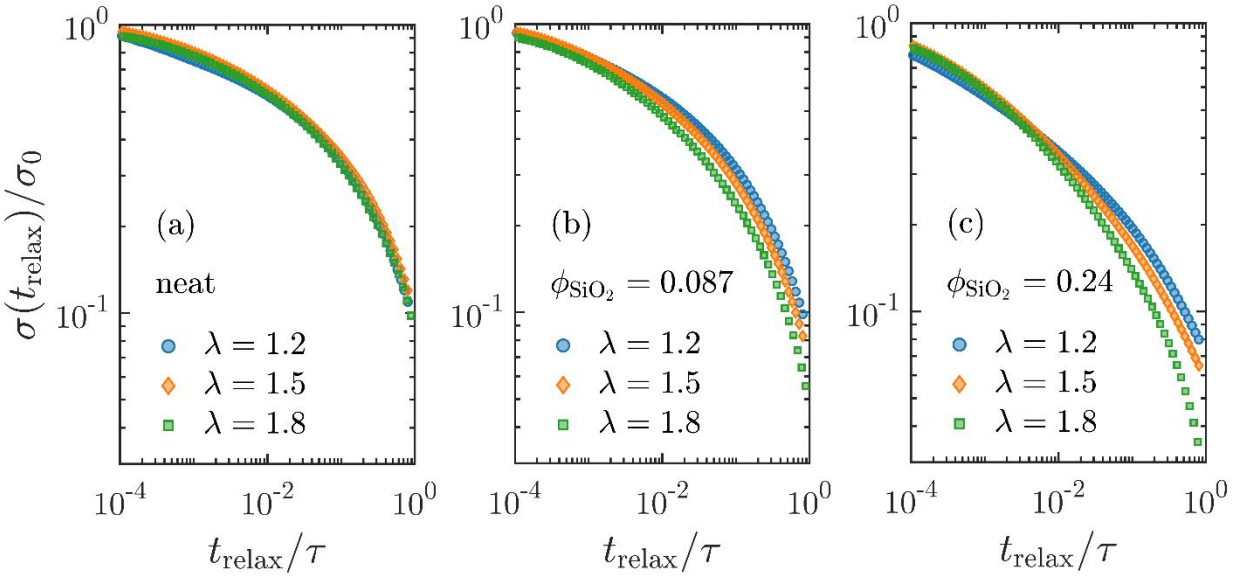


**Figure 4.** Stress relaxation, $\sigma(t_{\rm relax})/\sigma_0$, with normalized time $t_{\rm relax}/\tau$, at different elongation ratios $\lambda = 1.2$, 1.5, and 1.8 of (a) neat PS, (b) PS8.7, and (c) PS24. The neat polymer shows identical stress relaxation, exhibiting linear response at $\lambda \leq 1.8$. Both PS8.7 and PS24 show noticeable acceleration in stress relaxation with elongation ratios, signifying the involvement of nonlinear relaxation dynamics in PNCs.

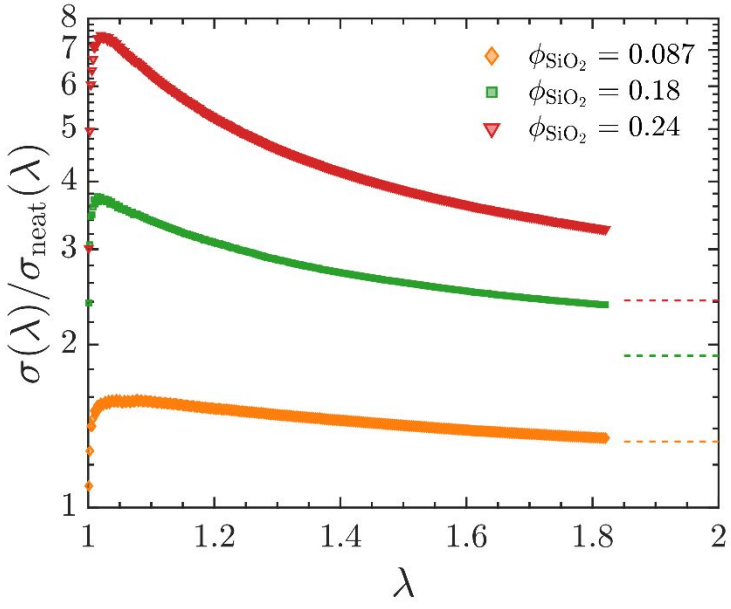


**Figure 5.** Reinforcement factor, $X \equiv \sigma(\lambda)/\sigma_{\rm neat}(\lambda)$, during step uniaxial extension. Dashed lines: reinforcement factor $X$ predicted by the Guth-Gold equation: $X = 1 + 2.5\phi_{\rm SiO_2} + 14.1\phi_{\rm SiO_2}^2$.

**Small-angle x-ray scattering (SAXS)**

The scattering intensities $I(Q)$ of the undeformed PNCs in SAXS measurements are shown in **Figure 6**. Using the form factor formula for a spherical particle, it is easy to verify that the Porod power-law scattering ($\sim Q^{-4}$) at high $Q$ ($\approx 0.1$ Å$^{-1}$) originates from the nanoparticle-polymer interface. On the other hand, the second power-law regime at low $Q$ ($\approx 0.01$ Å$^{-1}$) is associated with the interface between polymers and soft agglomerates of nanoparticles[79-81]. The soft agglomerates are different from hard agglomerates in filled elastomers[23] formed through sintering of the primary nanoparticles. Such multiple Porod regions in small-angle scattering have been widely observed in PNCs[79, 81, 82]. The observation of large-scale aggregates (or agglomerates) in SAXS is consistent with the strong mechanical reinforcement revealed by linear viscoelastic measurements (**Figure 2**), as well as scanning electron microscopy (SEM) measurements (inset of **Figure 6**). Although it is clear that large-scale aggregates are present in PNCs, detailed analyses of the NP aggregates are beyond the scope of the current study. As discussed in a following section, the lack of quantitative information about NP aggregations does not affect discussions of polymer dynamics during stress relaxation, since the microstructures of PNCs remain unchanged within the experimental time scale.

**Figure 7** presents the 2D SAXS spectra of the undeformed and deformed PNCs at different stages of the stress relaxation. Interestingly, *little* difference is observed for the SAXS spectra of different samples, regardless of the particle concentration, deformation state, and duration of stress relaxation. The lack of local NP structural changes is intriguing and highlights the important decoupling of the nanoscale nanoparticle rearrangement from macroscopic deformation. This is different from previous SAXS measurements of PMMA/$SiO_2$ nanocomposites with affine deformation of individual nanoparticles[83]. The strong decoupling between macroscopic

deformation and local structural anisotropy of the nanoparticle phase is further confirmed by quantitative analysis using the spherical harmonic expansion technique, which we shall discuss later. Both our rheological data (**Figure 3**) and previous investigations indicate that the soft agglomerates of nanoparticles could break up at large strains[24, 41, 80, 81, 84]. However, the negligible changes in the SAXS revealed that "local" structures of PNCs appear to be unaltered during stress relaxation at all $Q$s probed by SAXS.

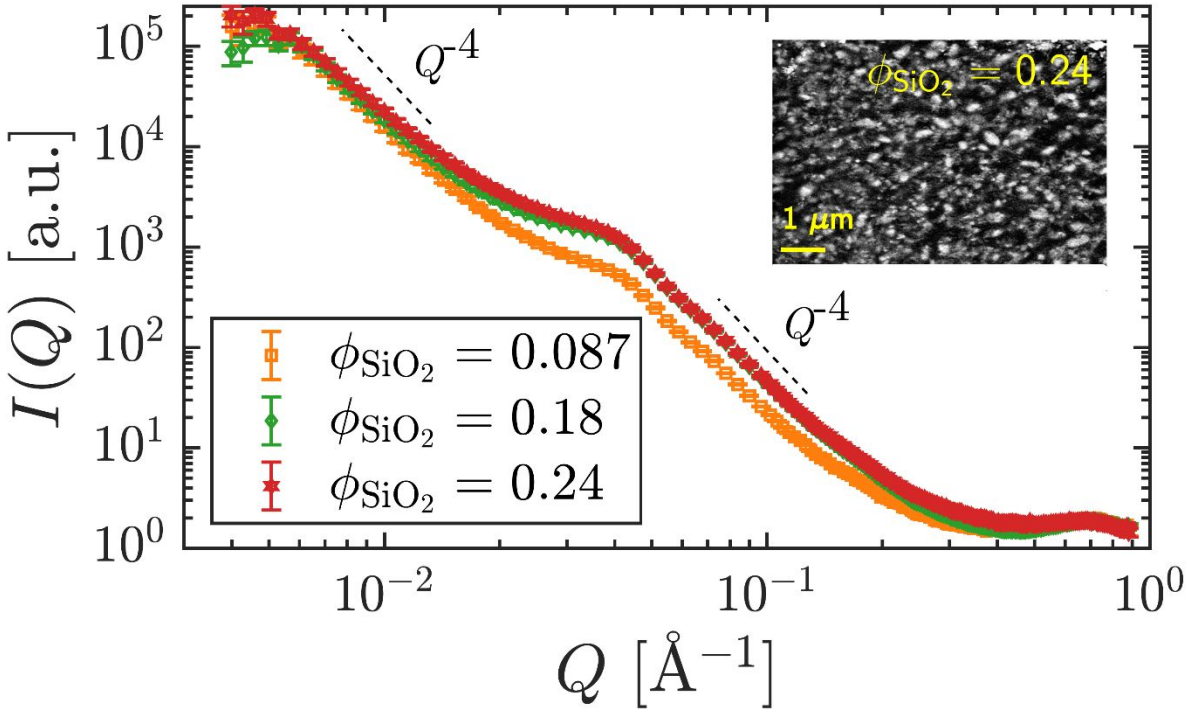


**Figure 6.** SAXS spectra of the undeformed PNCs. The inset shows an SEM image of the PS24 sample ($\phi_{SiO_2} = 0.24$) with large-size NP agglomerations (the bright regions). The dark region in the inset image is the polymer phase.

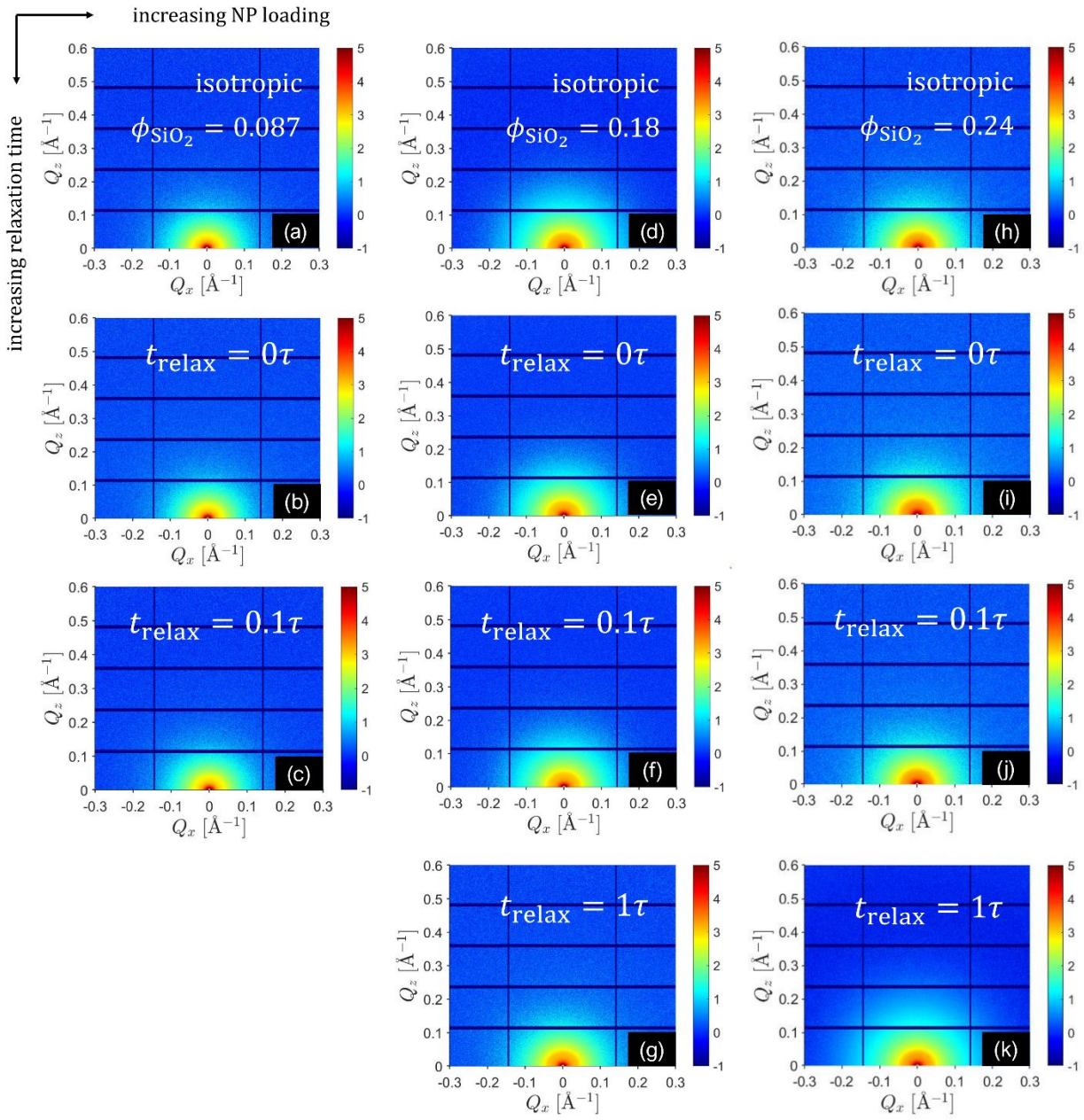


**Figure 7.** 2D SAXS spectra of PS/$SiO_2$ PNCs. (a)-(c): PS8.7. (d)-(g): PS18. (h)-(k): PS24. The color map presents $\log_{10}I(Q)$ on a linear scale.

**Small-angle neutron scattering (SANS)**

**Zero average contrast (ZAC).** In principle, the single-chain structure factor of the polymer $S(\mathbf{Q})$ can be obtained from SANS measurements under the ideal ZAC condition, namely, $\phi_D\rho_D + \phi_H\rho_H$

$-\rho_0 = 0$, as detailed in the Technical Background Section. By knowing the relevant atomic coherent scattering lengths[85] and material densities, the appropriate H/D ratio for the ZAC SANS experiment can be theoretically calculated and experimentally identified. A series of PNCs with a fixed NP loading but different H/D ratios [from 0.35:0.65 (CM1) to 0.90:0.10 (CM7)] were prepared (see the Materials and Methods Section for details). This covers a range of average SLD, $\rho_{\mathrm{p}} = \phi_{\mathrm{D}}\rho_{\mathrm{D}} + \phi_{\mathrm{H}}\rho_{\mathrm{H}}$, from $4.48 \times 10^{-6}\text{Å}^{-2}$ to $1.83 \times 10^{-6}\text{Å}^{-2}$ for the polymer phase, while the SLD of the nanoparticle $\rho_0 \approx 3.41 \times 10^{-6}\text{Å}^{-2}$ if the mass density of the silica particle is 2.16 g/cm$^3$. The results of SANS measurements on these samples are shown in **Figure 8**, where both the absolute intensity $I(Q)$ and normalized intensity $I(Q)/(\phi_{\mathrm{H}}\phi_{\mathrm{D}}\phi_{\mathrm{p}})$ are presented. Under ideal ZAC condition, the normalized coherent scattering intensity of PNCs, $I(\mathbf{Q})/(\phi_{\mathrm{H}}\phi_{\mathrm{D}}\phi_{\mathrm{p}})$, should match that of the neat polymer [Eq. (4)]. In practice, achieving ideal ZAC in PNCs is challenging[53] as revealed in **Figure 8** with strong upturn in scattering at the $Q < 0.01\ \text{Å}^{-1}$, regardless of the H/D ratio of the matrix polymer. Various mechanisms have been speculated for the low $Q$ upturn, including the scattering of the filler clusters[36], the potential H/D demixing[86], interfacial polymer[59, 87, 88], and the presence of voids or defects[89]. Nevertheless, the best contrast matching is found in the samples with H/D $\approx$ 0.57:0.43 at $Q > 0.01\ \text{Å}^{-1}$.

**Figure 9a** presents the normalized scattering intensity $I(Q)/\phi_{\mathrm{p}}$ of PS8.7, PS18, PS24, and the neat polystyrene ($\phi_{\mathrm{p}} = 1$) with H/D ratio of 0.57:0.43 in the polymer phase. The scattering intensity of all the PNCs has an upturn at $Q < 0.01\ \text{Å}^{-1}$, and a small bump at $Q \approx 0.04\ \text{Å}^{-1}$ is observed for PS18 and PS24. To gain further insight into the structural features of the PNCs, the SANS and SAXS spectra are directly compared in **Figure 9b**. The SAXS data are vertically shifted so that the SANS and SAXS data are matched at low $Q$s. The result in **Figure 9b** suggests that low-$Q$ upturn in SANS may originate from the filler clusters in the PNCs. Moreover, the

"shoulder" of in SAXS spectrum seems to conincide with the "bump" around $Q{\sim}0.04$ Å$^{-1}$ in PS18 and PS24. Due to the uncertainties of the physical origin of the low $Q$ upturn in scattering and the technical challenges of ZAC of PNCs, we are only comfortable to analyze scattering at $Q > 0.01$ Å$^{-1}$, where reasonable ZAC is achieved. Given $\pi/R_G \approx 0.02$ Å$^{-1}$ of PNCs, our analysis focusing at $Q > 0.01$ Å$^{-1}$ covers the most relevant length scales for the chain dynamics. Moreover, as we shall demonstrate below, the slight "mismatch" at $Q{\sim}0.04$ Å$^{-1}$ appears to contribute only to the isotropic component ($S_0^0$) of the spherical harmonic expansion and the analysis of structural anisotropy (e.g., $S_2^0$) is thus unaffected. Since the focus of the current study is the polymer anisotropy, $S_2^0(Q)$, after a step deformation, the isotropic contributions leading to the shoulder peak at $Q{\sim}0.04$ Å$^{-1}$ should not affect our analysis. From this perspective, the spherical harmonic expansion analysis is well suited for quantitative analysis of the nonlinear dynamics of multicomponent polymeric materials, bypassing a number of non-trivial theoretical and technical challenges confronted in conventional analysis for deformed polymers.

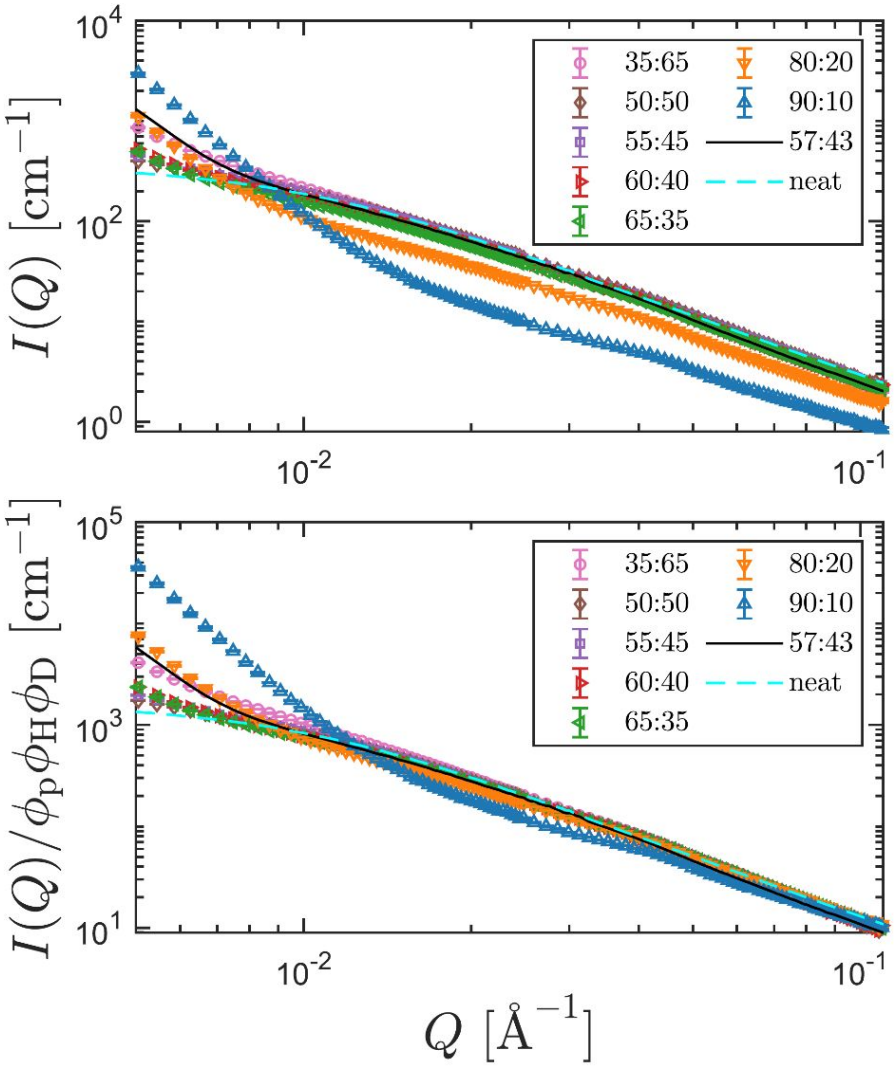


**Figure 8.** Results of SANS measurements of PS/SiO2 nanocomposites with different ratios of hydrogen and deuterium atoms (H/D). The nanoparticle loading is 8 v%. Black solid line: the result of PS8.7. Cyan dashed line: the result of PS0. (b) Normalized scattering intensity $I(Q)/(\phi_p\phi_H\phi_D)$, where $\phi_p$ is the volume fraction of polymer in the PNC, and $\phi_H$ and $\phi_D$ are respectively, the volume fractions of hydrogeneous and deuterated polystyrenes in the polymer phase.

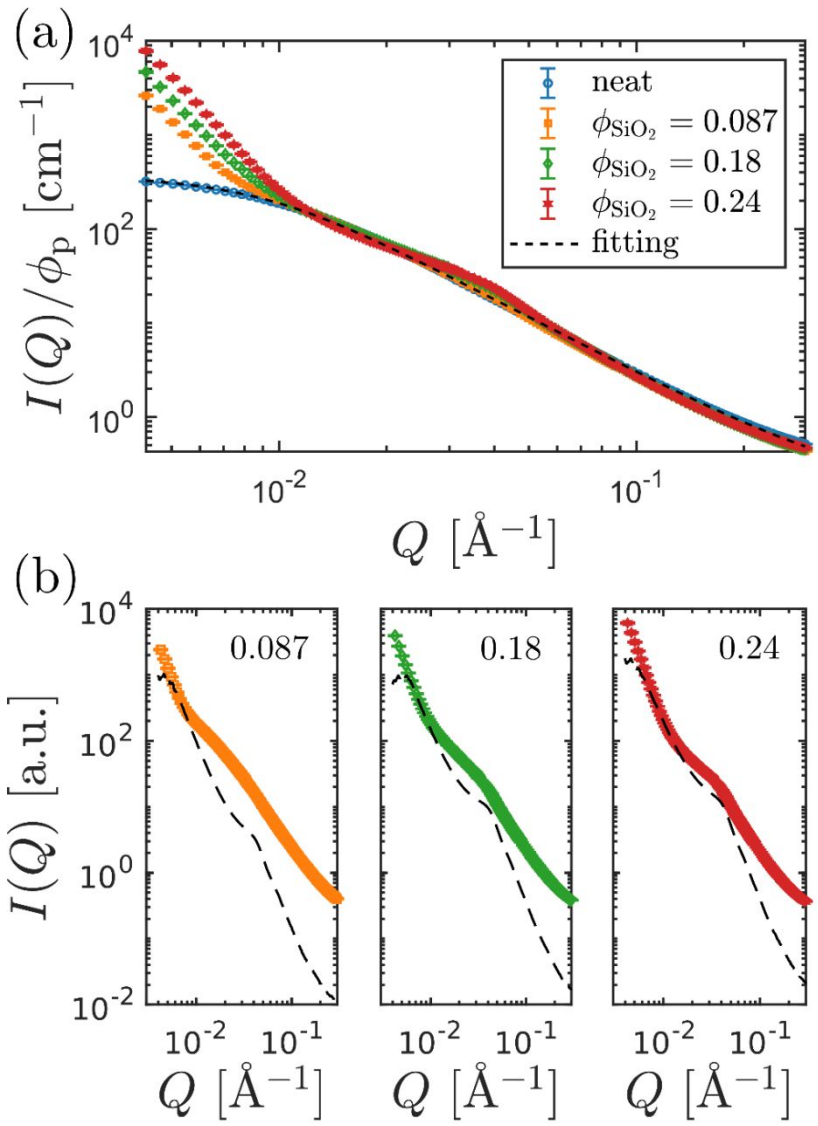


**Figure 9.** (a) Normalized SANS intensities $I(Q)/\phi_p$ of PS0, PS8.7, PS18, and PS24. Dashed line: fitting of the neat polystyrene SANS data with the Debye function: $I(Q) = I_0 g_D(Q^2 R_G^2) + I_{inc}$, where $g_D(x) = 2(e^{-x} - 1 + x)/x^2$. The fitting parameters are: $I_0 = 380.9 \pm 11.2$ cm$^{-1}$ (95% confidence interval), $R_G = 162.1 \pm 2.7$ Å (95% confidence interval), and $I_{inc} = 0.1582 \pm 0.0073$ cm$^{-1}$(95% confidence interval). (b) Comparison of SANS and SAXS spectra of PS8.7, PS18, and PS24. The SAXS curves are vertically shifted so that the SANS and SAXS data are matched at low $Q$s. Symbols: SANS data. Dashed lines: SAXS data.

**Neutron scattering of deformed PNCs. Figure 10** presents the 2D SANS spectra of the deformed polymers [PS0 (matrix polymer), PS8.7, PS18, and PS24] at $\lambda = 1.8$ during stress relaxation at

$t_{\text{relax}} = 0\ \tau$, 0.1 $\tau$, and 1.0 $\tau$. To properly compare the results at different particle concentrations, the absolute scattering intensity $I(Q)$ is normalized by the volume fraction of the polymer $\phi_{\text{p}}$. Immediately after the step uniaxial extension ($t_{\text{relax}} = 0\ \tau$), strong structural anisotropy is observed in all samples. As the tensile stress drops during relaxation, the anisotropy also decreases significantly with increasing time $t_{\text{relax}}$. Upon careful inspection, it appears that PNCs exhibit lower anisotropy than the neat polystyrene at a given relaxation time. To resolve such difference and quantitatively analyze the evolution of single-chain structure during stress relaxation, we resort to the spherical harmonic expansion technique. The results of the SHE analysis are presented in a next section.

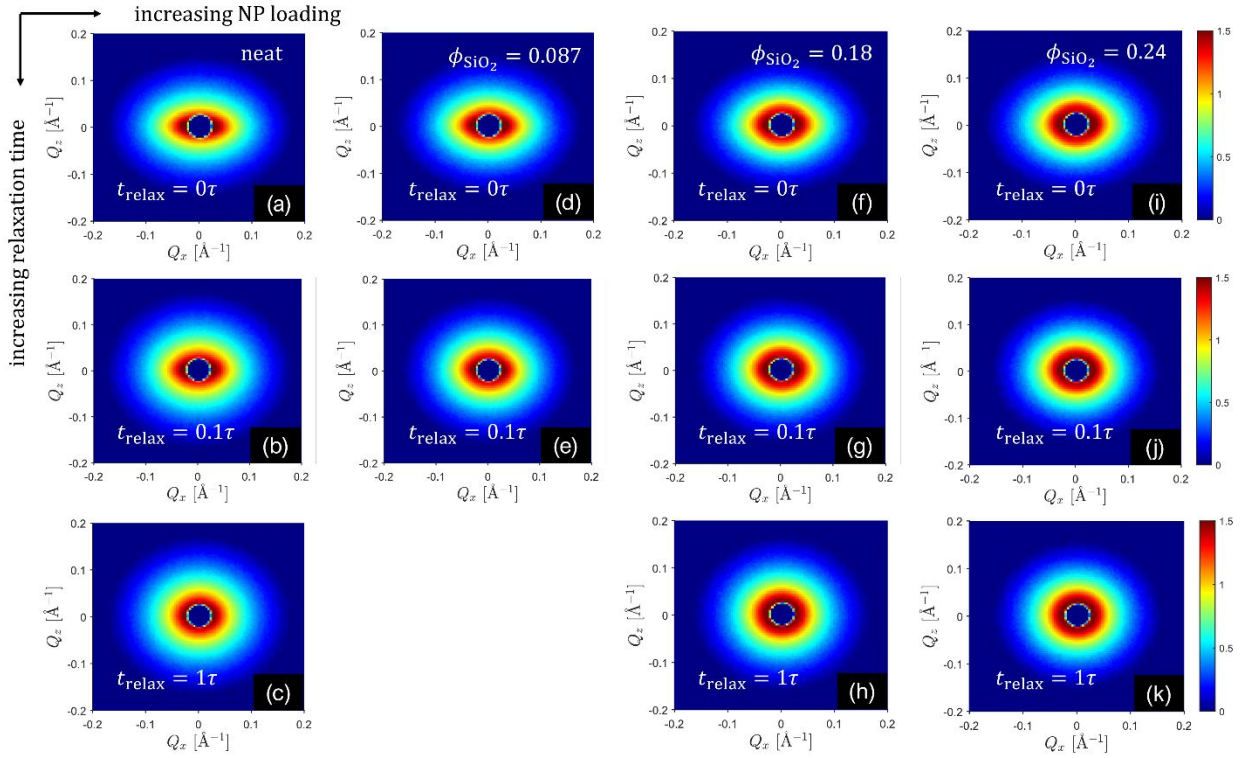


**Figure 10.** 2D SANS spectra of the deformed PS and PNCs. (a)-(c): results for PS0. (d) and (e): PS8.7. (f)-(h): PS18. (i)-(k): PS24. The color map presents $\log_{10}[I(Q)/\phi_{\text{p}}]$ on a linear scale.

## Discussions

### SHE analysis of structural anisotropy of deformed PNCs

An example of spherical expansion analysis of 2D SANS spectrum is given in **Figure 11**, where the expansion coefficients $S_0^0(Q)$, $S_2^0(Q)$, $S_4^0(Q)$, and $S_6^0(Q)$ of PS8.7 and the neat matrix are shown at $\lambda = 1.8$ and $t_{\text{relax}} = 0\,\tau$. Overall, the expansion coefficients of the two samples are almost identical, which is consistent with the "visual impression" from the 2D spectra (**Figure 10**) and in line with the previous result on PMMA/$SiO_2$ nanocomposites[39]. At moderate molecular deformation, the isotropic component $S_0^0(Q)Y_0^0(\theta)$ dominates the SANS spectrum. The contribution of higher order (degree) components becomes progressively smaller as $l$ increases. The spherical harmonic expansion method isolates the dominating contribution from the isotropic term, and thereby permits accurate analysis of structural anisotropy. We note that the leading anisotropic coefficient $S_2^0(Q)$ is connected to the microscopic tensile stress of the polymer chains[39, 67]. Therefore, our analysis of the structural relaxation dynamics will focus on the coefficient $S_2^0(Q)$.

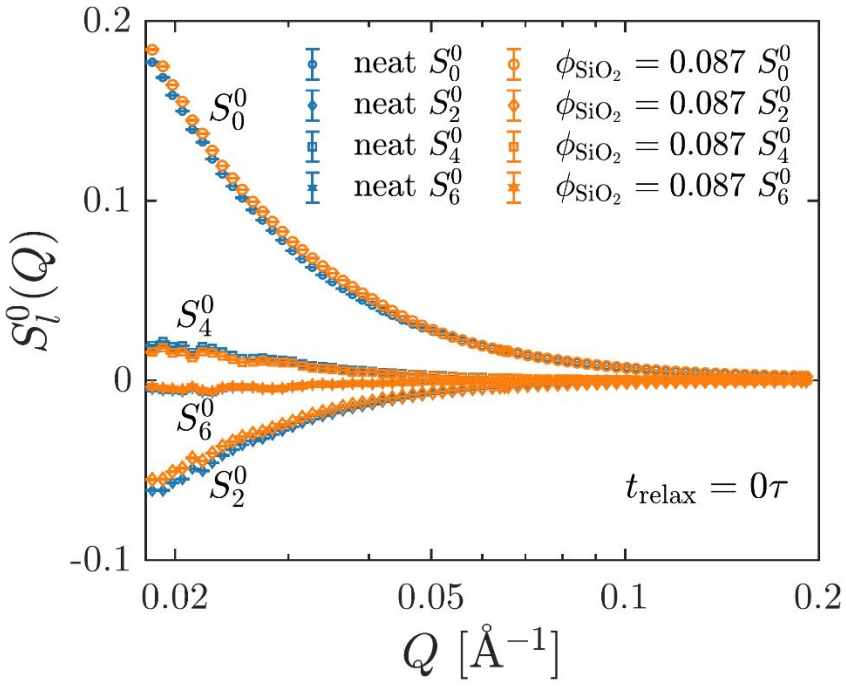

**Figure 11.** Spherical harmonic expansion coefficients $S_l^0(Q)$ of the single-chain structure factor of PS0 and PS8.7 immediately after the step uniaxial extension.

**Molecular mechanism of the high stress of PNCs at large deformation**

Strong mechanical enhancement was observed in PNCs in both the linear response region and at large deformation, as shown in **Figure 1**, **Figure 2**, and **Figure 3**. Two types of mechanisms are potentially responsible for the high mechanical strength of the PNCs beyond the hydrodynamic effect: molecular overstraining of the polymer chains[6] and elastic deformation of the NP aggregates (network)[25], both of which in principle can be analyzed by small-angle scattering techniques.

**Figure 12** shows the leading anisotropic expansion coefficient $-S_2^0(Q)$ of PS0, PS8.7, PS18, and PS24 from SANS during stress relaxation at $t_{\text{relax}} = 0\ \tau$, $0.1\ \tau$, and $1.0\ \tau$. Interestingly, the PNCs exhibit slightly smaller structural anisotropy than the neat polymer at all $Q$s, indicating the lack of enhancement in molecular orientation at all length scales from $l_K$ to $R_G$. Note that conventional 2D-SANS analyses[35, 37] of $R_G$ along with and perpendicular to the stretching direction provide little information on the structural anisotropy at length scales below $R_G$. From this perspective, the spherical harmonic expansion analysis offers a much more complete analysis for SANS spectra of deformed polymers.

Moreover, the degree of structural anisotropy reduction increases with particle loading. This result has not been previously reported. On the other hand, at $\lambda = 1.8$ and $t_{\text{relax}} = 0\ \tau$, the tensile stresses of PS8.7, PS18, and PS24 are 1.27, 2.5, and 3.3 times higher than the neat polymer, respectively. According to the strain amplification proposition[6], the average enhancement of local strain is at least $1 + 2.5\phi_{\text{SiO}_2}$, which yields amplification factors $X = 1.45$ and $X = 1.6$ for the $\phi_{\text{SiO}_2} = 0.18$ and $\phi_{\text{SiO}_2} = 0.24$ samples, respectively. While the reduction of structural anisotropy and

the enhancement of mechanical stress seems contradictory, a similar phenomenon was observed in our recent combined SANS and rheology investigation of a PMMA/$SiO_2$ nanocomposite[39]. The explanation lies in the hydrodynamic theory of mechanical reinforcement[1, 3, 4, 15, 16], where the presence of solid particles gives rise to a redistribution of local strain field but produces no enhancement of the average structural anisotropy[39]. Although this qualitative picture applies to the current PS/$SiO_2$ system, the reduction of anisotropy is beyond the reach of this simple explanation based on dilute suspensions and requires a more realistic treatment of the local strain field. Additionally, due to the presence of large-scale aggregates in PS/$SiO_2$, the potential stress contribution from the nanoparticle network should also be carefully considered to arrive at a clear understanding of the mechanical reinforcement of these highly-filled PNCs.

To further quantify the relaxation dynamics of polymer structural anisotropy[39, 67], the normalized expansion coefficients $S_2^0(Q;t_{\text{relax}})/S_2^0(Q;0)$ of all samples are shown in **Figure 13** for $t_{\text{relax}} = 0.01\,\tau,\ 0.03\,\tau,\ 0.1\,\tau,\ 0.3\,\tau,$ and $1.0\,\tau$. The quantity $\phi(Q;t) \equiv S_2^0(Q;t)/S_2^0(Q;0)$ can be interpreted as a $Q$-dependent structural anisotropy relaxation function[67], which characterizes the relative change of anisotropy at different length scales. Compared with the neat polymer matrix, the structural anisotropy relaxation is faster in PNCs at all $Q$s. This trend is consistent with the relaxation of mechanical stress $\sigma(t)/\sigma_0$ (inset of **Figure 3c**), which should not be surprising, considering the strong correlation between structural anisotropy and microscopic stress of polymers[67].

The spherical harmonic expansion technique is also applied to the 2D SAXS spectra (**Figure 7**) to quantify the structural changes of nanoparticles during stress relaxation. The expansion coefficients $I_0^0(Q)$ and $I_2^0(Q)$ of the scattering intensity $I(\mathbf{Q})$ are shown in **Figure 14**. Three prominent features are worth noting. First, the coefficients are almost identical, regardless of the

elapsed time during stress relaxation for all the PNC samples. Secondly, the SAXS spectra are dominated by the isotropic component of the expansion, in agreement with the cyclic symmetry of the 2D spectra (**Figure 7**). Lastly, weak structural anisotropy can be detected at low $Q$s, even for the undeformed samples. Because of the extremely slow diffusion of NPs in the highly viscous polymer matrix, $\tau \approx \frac{6\pi\eta R_{NP}^2}{k_B T} \sim 11\ days$ at $T = 393\ K$, the distortion of the large-scale structure of NP agglomerates during molding cannot be fully relaxed under normal experimental conditions. Note that the shear and Young's moduli of $SiO_2$ nanoparticles are around 30 GPa and 70 GPa, respectively[43]. Thus, negligible elastic deformation of $SiO_2$ nanoparticles is expected during molding and stretching. This further supports the conclusion that the minor differences of expansion coefficients at low $Q$s should be mainly associated with the initial state imparted by sample preparation, rather than a result of the deformation or the subsequent relaxation. Ideally, *in-operando* measurements capable of characterizing large-scale structures, such as rheo-USAXS, *in-situ* atomic force microscopy, *in-situ* SEM, and *in-situ* TEM, could be employed to quantify the detailed microstructure rearrangement of PNCs at deformation or during stress relaxation. However, applications of these *in-situ* microscopy methods and rheo-USAXS encounter technical challenges associated with sample preparations, measurements, and data interpretation[90-93]. Nevertheless, **Figure 14** indicates that the local structures of the NP dispersion remain largely unchanged *during the stress relaxation*. Given the full relaxation of the tensile stress at long time scales for all PNCs (**Figure 3**), one may thus infer that the short-range NP-NP interactions do not make any significant contribution to the total stress. Combining the rheological, SANS, and SAXS results, we conclude that the mechanical reinforcement mechanism in these PS/$SiO_2$ nanocomposites is like that of the PMMA/$SiO_2$ system[39]: a redistribution of strain field in the vicinity of nanoparticles, which is hydrodynamic in nature.

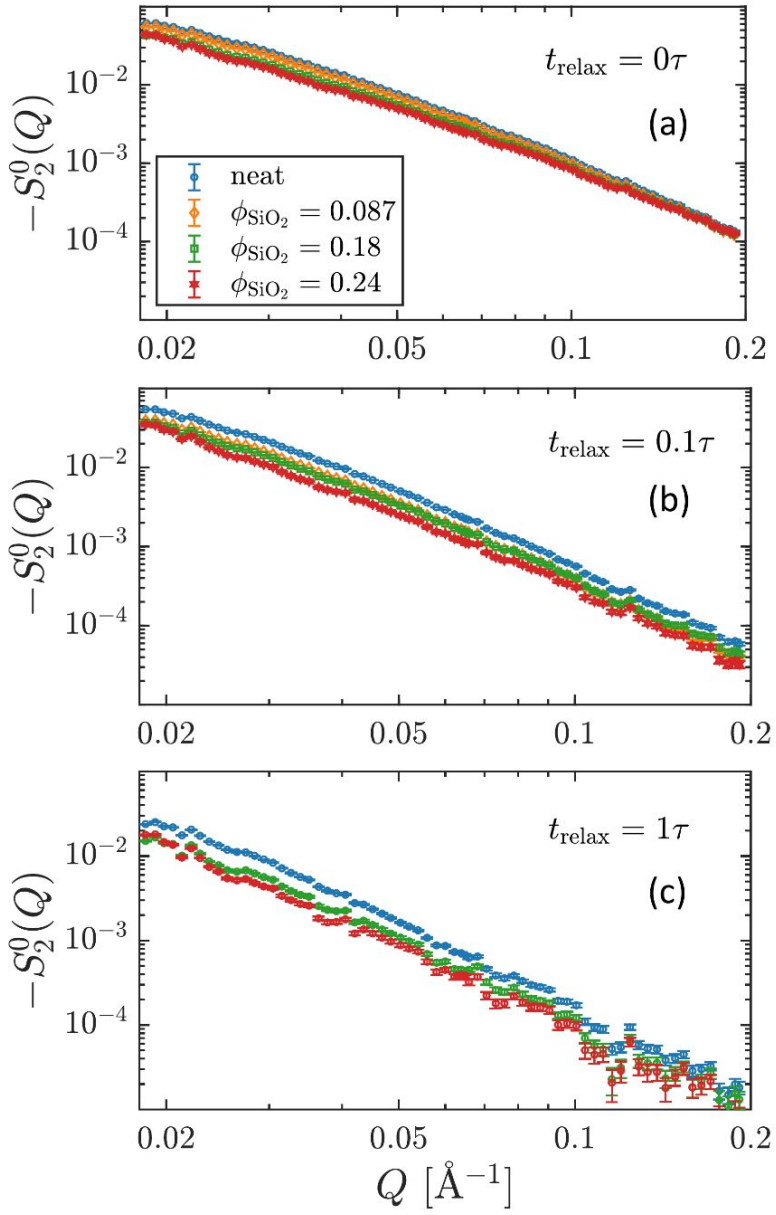


**Figure 12.** Leading anisotropic expansion coefficient $S_2^0(Q)$ of the deformed PS and PNCs at various stages of stress relaxation: (a) $t_{\mathrm{relax}} = 0\tau$, (b) $t_{\mathrm{relax}} = 0.1\tau$, and (c) $t_{\mathrm{relax}} = 1\tau$.

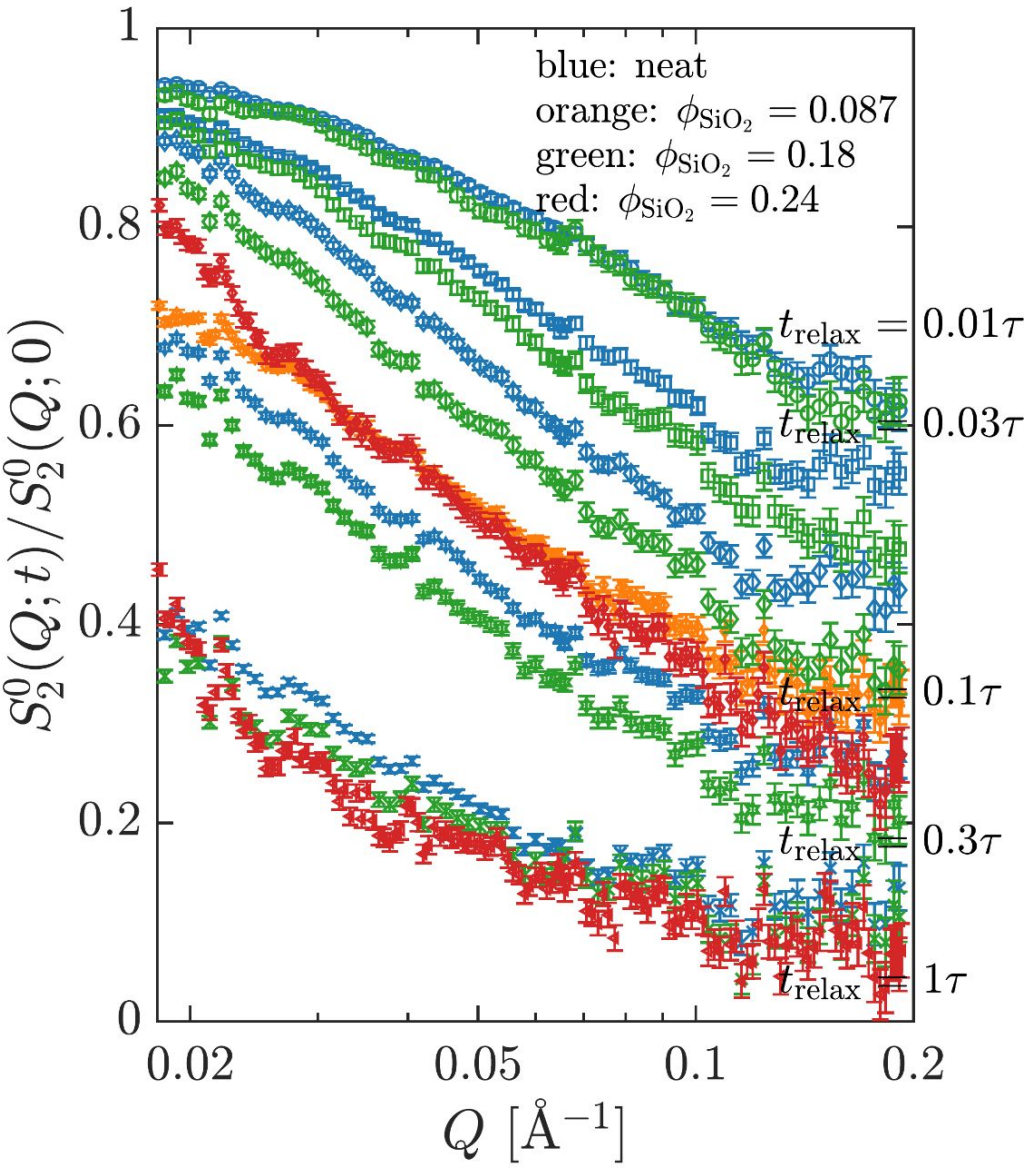


**Figure 13.** Relaxation of structural anisotropy of the deformed PS and PNCs. Here, $S_2^0(Q;0)$ is the leading anisotropic spherical harmonic expansion coefficient immediately after the step extension, i.e., at $t_{relax} = 0$. For the neat polymer and the PNC with $\phi_{SiO_2} = 0.18$, the data at five different relaxation times $t_{relax} = 0.01, 0.03, 0.1, 0.3$, and $1\tau$ are presented. For the PNC with $\phi_{SiO_2} = 0.087$, only the data at $t_{relax} = 0.1\tau$ is available. The data for the PNC with $\phi_{SiO_2} = 0.24$ are at two different relaxation times $t_{relax} = 0.1\tau$ and $t_{relax} = 1\tau$.

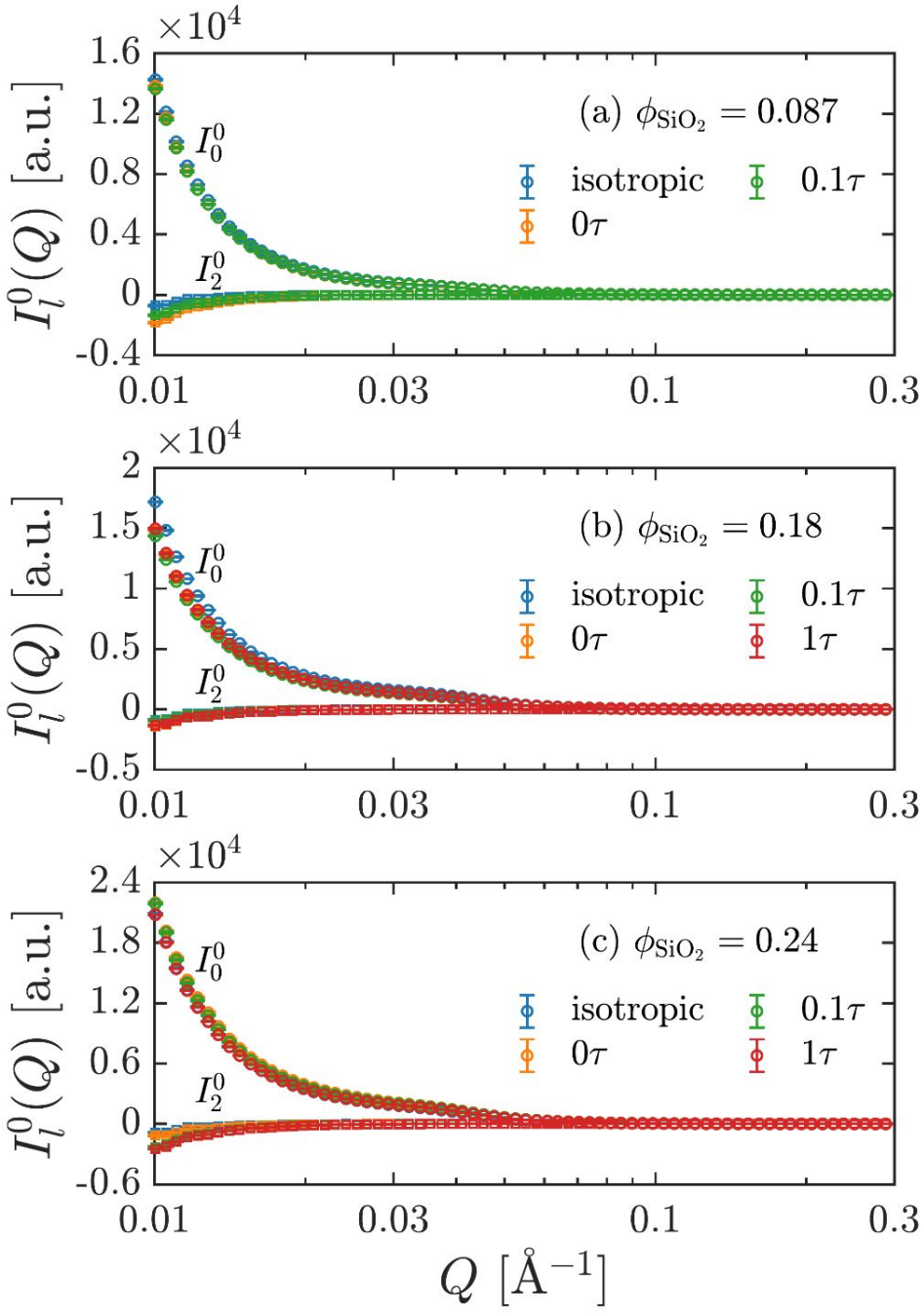


**Figure 14.** Spherical harmonic expansion coefficients $I_l^0(Q)$ obtained from the 2D SAXS spectra. PNC with (a) $\phi_{SiO_2} = 0.087$. (b) $\phi_{SiO_2} = 0.18$. (c) $\phi_{SiO_2} = 0.24$. Circles: $I_0^0(Q)$. Squares: $I_2^0(Q)$.

**Reduction of structural anisotropy and acceleration of relaxation dynamics**

One noticeable difference between the current PS/$SiO_2$ nanocomposites and the previous PMMA/$SiO_2$ system[39] is the accelerated stress and structural anisotropy relaxations in the PS/$SiO_2$ PNCs. In both cases, a step uniaxial strain is applied to the neat polymer and the PNCs. However, the dispersion of NPs is poor in the PS and NP concentrations as high as 24v% are investigated. It is not unreasonable to assume that the disturbance ("redistribution") of the local strain field is substantially larger in the highly filled PS/$SiO_2$ nanocomposites. For entangled polymer melts, the stress relaxation behavior below a critical step strain of $\lambda \approx 1.8$ is essentially linear as shown in **Figure 4**[65, 78, 94]. At low NP loading (PS8.7), the local strain field is not substantially distorted and the *average* relaxation dynamics of the PNC fall closely the linear response of the neat matrix polymer. By contrast, when the disturbance of the strain field is large (PS24), polymers in regions of significantly enhanced local strains are driven into deep nonlinear response. As a result, the average relaxation dynamics, in this case, become accelerated[78, 94] (**Figures 3** and **4**). Therefore, the hydrodynamic effect of NPs on the distortion of local strain field plays a critical role in the accelerated stress relaxation of deformed PNCs.

Another interesting observation is the reduced structural anisotropy [$S_2^0(Q)$] in the deformed PNCs compared with the neat matrix polymer (**Figure 12**). This difference underscores the significant influence of particle dispersion state on the local strain field. In the dilute limit, the classical hydrodynamic theory of mechanical reinforcement predicts a redistribution of strain field near a spherical particle with no enhancement of the *average* strain in the bulk. While this picture is in accordance with the result from PMMA/$SiO_2$ nanocomposites, it cannot explain the slight reduction of anisotropy in the PS/$SiO_2$ system. It is important to recognize that the relation between structural anisotropy and local strain is approximately linear only in the small deformation limit[39],

and magnitude of anisotropy [$S_2^0(Q)$] might saturate at large deformation. When the disturbance of the local strain field is large, as we may already conclude from the accelerated relaxation dynamics, the nonlinear relation between anisotropy and strain should lead to a reduction of the average expansion coefficient (anisotropy). In addition, two other factors may affect the local strain field in the PS/$SiO_2$ nanocomposites. One is the presence of considerable NP aggregates, which can promote the formation of occluded polymers. However, our SANS results cannot be fully described by the recently proposed network model,[95] with the assumption of presence of occluded polymers. Additionally, as discussed in the Results Section, the volume fraction of the occluded polymer in all the PNCs should be less than 10% at $\lambda = 1.8$. Given the strong accelerated stress relaxation of PNCs (**Figure 3** and **Figure 4**) and the more than 10% difference in $S_2^0$ between neat PS and PS18 and PS24 (**Figure 12**), the occluded polymer should play only a secondary role in the reduction in the structural anisotropy. The other is the large fraction of "interfacial layer polymers" at high NP loadings[42, 43, 96-102], including polystyrene on silica and other oxides[103, 104]. Extensive experimental and computational studies have suggested that the structure and dynamics of polymers in the vicinity of a nanoparticle can be substantially different from those in the bulk[99, 105-110]. A detailed understanding of the local strain fields at the interface during deformation, however, is beyond the scope of this work and requires further theoretical and computational studies. Nevertheless, it is helpful to point out that our recent nonlinear rheological measurements suggest that the interfacial layer polymers do not seem to play a leading role in the mechanical reinforcement of PNCs at large deformation[41].

## Conclusion

In summary, the relaxation dynamics of deformed polystyrene/silica nanocomposites are investigated by the combination of small-angle x-ray scattering, small-angle neutron scattering,

and rheology. Applications of the spherical harmonic expansion technique and the zero-average-contrast approach permit quantitative SANS studies of the single-chain structure factor of the polymer matrix after a large step uniaxial deformation. While the nanoparticles enhance the mechanical stress in the linear viscoelastic regime and during the initial phase of step relaxation, reduced structural anisotropy and accelerated relaxation dynamics are observed in the polymer nanocomposites. We show that these observations can be rationalized with the hydrodynamic reinforcement picture when additional nonlinear effects associated with strain field redistribution are considered. Specifically, in the presence of large macroscopic deformation and local disturbance field, the reduction of structural anisotropy and acceleration of relaxation dynamics are results of the nonlinear response of entangled polymers and the nonlinear relation between polymer structural anisotropy and microscopic strain.

## Appendix

### Zero-average-contrast matching approach to polymer nanocomposites

In this appendix, we give a derivation of the scattering function of polymer nanocomposites consisting of nanoparticles, and hydrogenous and deuterated polymers of matching molecular weights, for the reader's convenience. By exposing the details of the derivation, potential challenges of achieving ideal ZAC condition can be better appreciated. According to the fundamental theorem of small-angle neutron scattering by incompressible liquids[50], the *unnormalized* scattering intensity can be expressed as:

$$I(\mathbf{Q}) = \sum_{\alpha} (v_\alpha \Delta\rho_\alpha)^2 S_{\alpha\alpha}(\mathbf{Q}) + \sum_{\alpha \neq \beta} (v_\alpha \Delta\rho_\alpha)(v_\beta \Delta\rho_\beta) S_{\alpha\beta}(\mathbf{Q}), \tag{11}$$

where $v_\alpha$ is the molecular volume of the species α, $\Delta\rho_\alpha$ is the corresponding contrast factor (scattering length density difference between the species α and the reference species), and $S_{\alpha\beta}(\mathbf{Q})$

is the partial structure factor, defined as $S_{\alpha\beta}(\mathbf{Q}) \equiv \sum_{m=1}^{N_\alpha}\sum_{n=1}^{N_\beta}\langle \exp[-i\mathbf{Q}\cdot(\mathbf{R}_m - \mathbf{R}_n)]\rangle$, with $\mathbf{R}_m$ being the position of the scattering unit $m$. In the case of the current PNC system, it is convenient to choose silica nanoparticles as the reference species. Therefore, $I(\mathbf{Q})$ can be written as:

$$I(\mathbf{Q}) = v_{\mathrm{H}}^2(\rho_{\mathrm{H}} - \rho_0)^2 S_{\mathrm{HH}}(\mathbf{Q}) + v_{\mathrm{D}}^2(\rho_{\mathrm{D}} - \rho_0)^2 S_{\mathrm{DD}}(\mathbf{Q}) + 2v_{\mathrm{H}}(\rho_{\mathrm{H}} - \rho_0)v_{\mathrm{D}}(\rho_{\mathrm{D}} - \rho_0)S_{\mathrm{HD}}(\mathbf{Q}), \tag{12}$$

where $\rho_{\mathrm{H}}$, $\rho_{\mathrm{D}}$, and $\rho_0$ are the scattering length densities of the hydrogenous polymers, deuterated polymers, and nanoparticles, respectively. Following the standard technique, we can decompose $S_{\mathrm{HH}}(\mathbf{Q})$ and $S_{\mathrm{DD}}(\mathbf{Q})$ into contributions from interchain and intrachain correlations:

$$S_{\mathrm{HH}}(\mathbf{Q}) = \phi MN^2 S_{\mathrm{HH,intra}}(\mathbf{Q}) + \phi^2 M^2 N^2 S_{\mathrm{HH,inter}}(\mathbf{Q}), \tag{13}$$

$$S_{\mathrm{DD}}(\mathbf{Q}) = (1-\phi)MN^2 S_{\mathrm{DD,intra}}(\mathbf{Q}) + (1-\phi)^2 M^2 N^2 S_{\mathrm{DD,inter}}(\mathbf{Q}), \tag{14}$$

where $\phi$ is the molar fraction of hydrogenous chains in the polymer phase (excluding the particles), $M$ is the total number of polymer chains, and $N$ is the chain length. In absence of isotopic effect, we have $S_{\mathrm{HH,intra}} = S_{\mathrm{DD,intra}}$ and $S_{\mathrm{HH,inter}} = S_{\mathrm{DD,inter}} = S_{\mathrm{HD,inter}}$. Additionally, it is reasonable to assume that $v_{\mathrm{H}} = v_{\mathrm{D}} = v$. The contributions from HH, DD, and HD correlations to $I(\mathbf{Q})$ are therefore respectively:

$$v^2(\rho_{\mathrm{H}} - \rho_0)^2\left[\phi MN^2 S_{\mathrm{intra}}(\mathbf{Q}) + \phi^2 M^2 N^2 S_{\mathrm{inter}}(\mathbf{Q})\right], \tag{15}$$

$$v^2(\rho_{\mathrm{D}} - \rho_0)^2\left[(1-\phi)MN^2 S_{\mathrm{intra}}(\mathbf{Q}) + (1-\phi)^2 M^2 N^2 S_{\mathrm{inter}}(\mathbf{Q})\right], \tag{16}$$

$$2v^2(\rho_{\mathrm{H}} - \rho_0)(\rho_{\mathrm{D}} - \rho_0)\phi(1-\phi)M^2 N^2 S_{\mathrm{inter}}(\mathbf{Q}). \tag{17}$$

After some arithmetic rearrangements, we find:

$$I(\mathbf{Q}) = v^2(\rho_{\mathrm{H}} - \rho_{\mathrm{D}})^2\phi(1-\phi)MN^2 S_{\mathrm{intra}}(\mathbf{Q}) + v^2[\phi\rho_{\mathrm{H}} + (1-\phi)\rho_{\mathrm{D}} - \rho_0]^2\left[MN^2 S_{\mathrm{intra}}(\mathbf{Q}) + M^2 N^2 S_{\mathrm{inter}}(\mathbf{Q})\right]. \tag{18}$$

Since $vMN = V_{\mathrm{p}}$ is the total volume of the polymers, the above result can be rewritten as:

$$\frac{I(\mathbf{Q})}{V} = (\rho_{\mathrm{H}} - \rho_{\mathrm{D}})^2 \phi(1-\phi)\frac{\phi_{\mathrm{p}}}{\nu_{\mathrm{chain}}} S_{\mathrm{intra}}(\mathbf{Q}) + [\phi\rho_{\mathrm{H}} + (1-\phi)\rho_{\mathrm{D}} - \rho_0]^2 \left[\frac{\phi_{\mathrm{p}}}{\nu_{\mathrm{chain}}} S_{\mathrm{intra}}(\mathbf{Q}) + V_{\mathrm{p}}\phi_{\mathrm{p}} S_{\mathrm{inter}}(\mathbf{Q})\right]. \quad (19)$$

The left-hand side of the equation is the volume normalized scattering intensity, which is the typical "absolute scattering intensity" given by a SANS instrument. Here, $V_{\mathrm{p}}$ is the total volume of the polymer phase, $\phi_{\mathrm{p}}$ is the volume fraction of the polymer phase in the PNC, and $\nu_{\mathrm{chain}}$ is the number density (per volume) of chains in the polymer phase. When the average contrast $\phi\rho_{\mathrm{H}} + (1-\phi)\rho_{\mathrm{D}} - \rho_0$ is zero, the second term on the right-hand side of Eq. (19) vanishes, and we have:

$$\frac{I(\mathbf{Q})}{V} = (\rho_{\mathrm{H}} - \rho_{\mathrm{D}})^2 \phi(1-\phi)\frac{\phi_{\mathrm{p}}}{\nu_{\mathrm{chain}}} S_{\mathrm{intra}}(\mathbf{Q}) = (b_{\mathrm{H}} - b_{\mathrm{D}})^2 \phi(1-\phi)\phi_{\mathrm{p}} n_{\mathrm{seg}} N S_{\mathrm{intra}}(\mathbf{Q}), \quad (A10)$$

where $n_{\mathrm{seg}}$ is the polymer segment density (per volume) in the polymer phase and $b_H = \rho_H \nu$ and $b_D = \rho_D \nu$ are the scattering length of the hydrogenous segment and the deuterated segment. We note that Eq. (A10) is identical to the well-known result for isotopically labeled polymer melts, except for the prefactor $\phi_{\mathrm{p}}$. In the main text, the volume normalized scattering intensity (absolute scattering intensity) is simply denoted by $I(\mathbf{Q})$; additionally, $S_{\mathrm{intra}}(\mathbf{Q})$ is the same as the single-chain structure factor and is abbreviated as $S(\mathbf{Q})$.

The derivation of Eq. (A10) relies on two main assumptions: incompressibility and ideal mixing of hydrogenous and deuterated chains. While the former assumption should hold well, deviations from the ideal mixing condition might be expected. In particular, it is well known that the structures of polymers near the nanoparticle surface can be strongly disturbed, leading to a breakdown of the simple assumption of spatial homogeneity in the polymer phase.

## Author Contributions

S.C. and Y. W. conceived the idea, designed the experiments, and supervised the research. R. S., J. Y., S. P., Y. L., X. Z., A. L., Y. W., and S. C. performed the experiments and collected the data. R. S., J. Y., Y. L., X. Z., Y. W., and S. C. analyzed the data. All authors participated in the writing.

## Conflicts of interest

There are no conflicts to declare.

## Acknowledgements

This work was supported, in part, by the Ralph E. Powe Junior Faculty Enhancement Awards from Oak Ridge Associated Universities (S.C.). Y.W. acknowledges support by the U.S. Department of Energy, Office of Science, Office of Basic Energy Sciences, Early Career Research Program Award KC0402010, under contract DE-AC05-00OR22725. Part of this work was performed at the Oak Ridge National Laboratory's Center for Nanophase Materials Sciences, which is a DOE Office of Science User Facility. The SAXS measurements were performed at Beamline 12-ID-B of Advanced Photon Source, a U.S. Department of Energy (DOE) Office of Science User Facility operated for the DOE Office of Science by Argonne National Laboratory under Contract No. DE-AC02-06CH11357. Access to NGB 30m SANS was provided by the Center for High Resolution Neutron Scattering, a partnership between the National Institute of Standards and Technology (NIST) and the National Science Foundation under Agreement No. DMR-1508249. Certain commercial equipment, instruments, or materials are identified in this document. Such identifications do not imply recommendation or endorsement by the NIST nor does it imply that the products identified are necessarily the best available for the purpose. We thank Matthew Melton for help on the SEM measurements.

## References


1. H. M. Smallwood, Limiting Law of the Reinforcement of Rubber, *J. Appl. Phys.* , 1944, **15**, 758-766.
2. E. Guth, Theory of Filler Reinforcement, *J. Appl. Phys.* , 1945, **16**, 20-25.
3. A. Einstein, *Investigations on the Theory of the Brownian Movement*, Dover Publications, U.S, 1956.
4. J. D. Eshelby and R. E. Peierls, The determination of the elastic field of an ellipsoidal inclusion, and related problems, *Proc. R. Soc. London, Ser. A*, 1957, **241**, 376-396.
5. H. Brenner, Dissipation of Energy due to Solid Particles Suspended in a Viscous Liquid, *The Physics of Fluids*, 1958, **1**, 338-346.
6. L. Mullins and N. R. Tobin, Stress softening in rubber vulcanizates. Part I. Use of a strain amplification factor to describe the elastic behavior of filler-reinforced vulcanized rubber, *J. Appl. Polym. Sci.* , 1965, **9**, 2993-3009.
7. D. J. Jeffrey and A. Acrivos, The rheological properties of suspensions of rigid particles, *AlChE J.* , 1976, **22**, 417-432.
8. G. K. Batchelor, The effect of Brownian motion on the bulk stress in a suspension of spherical particles, *J. Fluid Mech.* , 1977, **83**, 97-117.
9. G. R. Hamed, Reinforcement of Rubber, *Rubber Chem. Technol.* , 2000, **73**, 524-533.
10. G. Huber and T. A. Vilgis, On the Mechanism of Hydrodynamic Reinforcement in Elastic Composites, *Macromolecules*, 2002, **35**, 9204-9210.
11. C. G. Robertson, R. Bogoslovov and C. M. Roland, Structural arrest and thermodynamic scaling in filler-reinforced polymers, *Rubber Chem. Technol.* , 2009, **82**, 202-213.
12. J. W. Bullard, A. T. Pauli, E. J. Garboczi and N. S. Martys, A comparison of viscosity–concentration relationships for emulsions, *J. Colloid Interface Sci.* , 2009, **330**, 186-193.
13. H. Hasimoto, A Sphere Theorem on the Stokes Equation for Axisymmetric Viscous Flow, *J. Phys. Soc. Jpn.* , 1956, **11**, 793-797.
14. G. K. Batchelor, The stress system in a suspension of force-free particles, *J. Fluid Mech.* , 1970, **41**, 545-570.
15. A. T. Chwang and T. Y.-T. Wu, Hydromechanics of low-Reynolds-number flow. Part 2. Singularity method for Stokes flows, *J. Fluid Mech.* , 1975, **67**, 787-815.
16. E. Guazzelli and J. F. Morris, *A Physical Introduction to Suspension Dynamics*, Cambridge University Press, 2011.
17. J. Mewis and N. J. Wagner, *Colloidal Suspension Rheology*, Cambridge University Press, 2012.
18. M. M. Rueda, M.-C. Auscher, R. Fulchiron, T. Périé, G. Martin, P. Sonntag and P. Cassagnau, Rheology and applications of highly filled polymers: A review of current understanding, *Prog. Polym. Sci.* , 2017, **66**, 22-53.
19. Y. Song and Q. Zheng, Concepts and Conflicts in Nanoparticles Reinforcement to Polymers beyond Hydrodynamics, *Prog. Mater Sci.* , 2016, **84**, 1-58.
20. Y. Song and Q. Zheng, A Guide for Hydrodynamic Reinforcement Effect in Nanoparticle-filled Polymers, *Crit. Rev. Solid State Mater. Sci.* , 2016, **41**, 318-346.
21. T. A. Witten, M. Rubinstein and R. H. Colby, Reinforcement of rubber by fractal aggregates, *J. Phys. II France*, 1993, **3**, 367-383.
22. S. M. Smith and D. S. Simmons, Horizons for design of filled rubber informed by molecular dynamics simulation, *Rubber Chem. Technol.* , 2017, **90**, 238-263.

23. T. A. Vilgis, G. Heinrich and M. Klüppel, *Reinforcement of Polymer Nano-Composites: Theory, Experiments and Applications*, Cambridge University Press, Cambridge, 2009.
24. M. Klüppel and G. Heinrich, Fractal Structures in Carbon Black Reinforced Rubbers, *Rubber Chem. Technol.* , 1995, **68**, 623-651.
25. G. Heinrich and M. Klüppel, Recent Advances in the Theory of Filler Networking in Elastomers, in *Filled Elastomers Drug Delivery Systems*, Springer Berlin Heidelberg, Berlin, Heidelberg, 2002, DOI: 10.1007/3-540-45362-8_1, pp. 1-44.
26. B. M. Yavitt, D. Salatto, Y. Zhou, Z. Huang, M. Endoh, L. Wiegart, V. Bocharova, A. E. Ribbe, A. P. Sokolov, K. S. Schweizer and T. Koga, Collective Nanoparticle Dynamics Associated with Bridging Network Formation in Model Polymer Nanocomposites, *ACS Nano*, 2021, **15**, 11501-11513.
27. Q. Chen, S. Gong, J. Moll, D. Zhao, S. K. Kumar and R. H. Colby, Mechanical Reinforcement of Polymer Nanocomposites from Percolation of a Nanoparticle Network, *ACS Macro Letters*, 2015, **4**, 398-402.
28. D. Zhao, S. Ge, E. Senses, P. Akcora, J. Jestin and S. K. Kumar, Role of Filler Shape and Connectivity on the Viscoelastic Behavior in Polymer Nanocomposites, *Macromolecules*, 2015, **48**, 5433-5438.
29. Z. Zhu, T. Thompson, S.-Q. Wang, E. D. von Meerwall and A. Halasa, Investigating Linear and Nonlinear Viscoelastic Behavior Using Model Silica-Particle-Filled Polybutadiene, *Macromolecules*, 2005, **38**, 8816-8824.
30. J. Jancar, J. F. Douglas, F. W. Starr, S. K. Kumar, P. Cassagnau, A. J. Lesser, S. S. Sternstein and M. J. Buehler, Current issues in research on structure-property relationships in polymer nanocomposites, *Polymer*, 2010, **51**, 3321-3343.
31. S. K. Kumar, V. Ganesan and R. A. Riggleman, Perspective: Outstanding theoretical questions in polymer-nanoparticle hybrids, *J. Chem. Phys.* , 2017, **147**, 020901.
32. J. E. Mark, B. Erman and C. M. Roland, *The Science and Technology of Rubber*, Academic Press, 4th edn., 2013.
33. J. Domurath, M. Saphiannikova and G. Heinrich, The concept of hydrodynamic amplification in filled elastomers, *Kautschuk und Gummi Kunststoffe*, 2017, **70**, 40-43.
34. J. Wang, Y. Guo, W. Yu, C. X. Zhou and P. Steeman, Linear and nonlinear viscoelasticity of polymer/silica nanocomposites: an understanding from modulus decomposition, *Rheol. Acta* 2016, **55**, 37-50.
35. S. Westermann, M. Kreitschmann, W. Pyckhout-Hintzen, D. Richter, E. Straube, B. Farago and G. Goerigk, Matrix Chain Deformation in Reinforced Networks: a SANS Approach, *Macromolecules*, 1999, **32**, 5793-5802.
36. A. Botti, W. Pyckhout-Hintzen, D. Richter, V. Urban and E. Straube, A microscopic look at the reinforcement of silica-filled rubbers, *J. Chem. Phys.* , 2006, **124**, 174908.
37. N. Jouault, F. Dalmas, S. Said, E. Di Cola, R. Schweins, J. Jestin and F. Boué, Direct small-angle-neutron-scattering observation of stretched chain conformation in nanocomposites: More insight on polymer contributions in mechanical reinforcement, *Phys. Rev. E*, 2010, **82**, 031801.
38. R. Pérez-Aparicio, M. Schiewek, J. L. Valentín, H. Schneider, D. R. Long, M. Saphiannikova, P. Sotta, K. Saalwächter and M. Ott, Local Chain Deformation and Overstrain in Reinforced Elastomers: An NMR Study, *Macromolecules*, 2013, **46**, 5549-5560.

39. R. Sun, M. Melton, N. Safaie, R. C. Ferrier, S. Cheng, Y. Liu, X. Zuo and Y. Wang, Molecular View on Mechanical Reinforcement in Polymer Nanocomposites, *Phys. Rev. Lett.* , 2021, **126**, 117801.
40. J. Yang, M. Melton, R. Sun, W. Yang and S. Cheng, Decoupling the Polymer Dynamics and the Nanoparticle Network Dynamics of Polymer Nanocomposites through Dielectric Spectroscopy and Rheology, *Macromolecules*, 2020, **53**, 302-311.
41. R. Sun, M. Melton, X. Zuo and S. Cheng, Nonmonotonic Strain Rate Dependence on the Strain Hardening of Polymer Nanocomposites, *ACS Macro Letters*, 2020, **9**, 1224-1229.
42. S. Cheng, A. P. Holt, H. Wang, F. Fan, V. Bocharova, H. Martin, T. Etampawala, B. T. White, T. Saito, N.-G. Kang, M. D. Dadmun, J. W. Mays and A. P. Sokolov, Unexpected Molecular Weight Effect in Polymer Nanocomposites, *Phys. Rev. Lett.* , 2016, **116**, 038302.
43. S. Cheng, V. Bocharova, A. Belianinov, S. Xiong, A. Kisliuk, S. Somnath, A. P. Holt, O. S. Ovchinnikova, S. Jesse, H. Martin, T. Etampawala, M. Dadmun and A. P. Sokolov, Unraveling the Mechanism of Nanoscale Mechanical Reinforcement in Glassy Polymer Nanocomposites, *Nano Lett.* , 2016, **16**, 3630-3637.
44. M. Jhalaria, A. M. Jimenez, R. Mathur, M. C. Tekell, Y. Huang, S. Narayanan, B. C. Benicewicz and S. K. Kumar, Long-Term Aging in Miscible Polymer Nanocomposites, *Macromolecules*, 2022, **55**, 4502-4515.
45. J. D. Ferry, *Viscoelastic properties of polymers*, Wiley, New York, 1980.
46. L. J. Fetters, D. J. Lohse, D. Richter, T. A. Witten and A. Zirkel, Connection between polymer molecular weight, density, chain dimensions, and melt viscoelastic properties, *Macromolecules*, 1994, **27**, 4639-4647.
47. Y. Wang and S.-Q. Wang, Salient Features in Uniaxial Extension of Polymer Melts and Solutions: Progressive Loss of Entanglements, Yielding, Non-Gaussian Stretching, and Rupture, *Macromolecules*, 2011, **44**, 5427-5435.
48. J. P. Cotton, D. Decker, H. Benoit, B. Farnoux, J. Higgins, G. Jannink, R. Ober, C. Picot and J. des Cloizeaux, Conformation of Polymer Chain in the Bulk, *Macromolecules*, 1974, **7**, 863-872.
49. A. Z. Akcasu, G. C. Summerfield, S. N. Jahshan, C. C. Han, C. Y. Kim and H. Yu, Measurement of single chain neutron scattering in concentrated polymer solutions, *J. Polym. Sci., Polym. Phys. Ed*, 1980, **18**, 863-869.
50. J. S. Higgins and H. Benoît, *Polymers and Neutron Scattering*, Clarendon Press, 1994.
51. Y. Wang, W. Wang, K. Hong, C. Do and W.-R. Chen, Quantitative examination of a fundamental assumption in small-angle neutron scattering studies of deformed polymer melts, *Polymer*, 2020, **204**, 122698.
52. J. T. Koberstein, Small-angle neutron scattering from two-phase polymeric systems, *J. Polym. Sci., Polym. Phys. Ed*, 1982, **20**, 593-602.
53. A. Botti, W. Pyckhout-Hintzen, D. Richter, V. Urban, E. Straube and J. Kohlbrecher, Silica filled elastomers: polymer chain and filler characterization in the undeformed state by a SANS–SAXS approach, *Polymer*, 2003, **44**, 7505-7512.
54. B. Hammouda, SANS from homogeneous polymer mixtures: A unified overview, in *Polymer Characteristics*, Springer Berlin Heidelberg, Berlin, Heidelberg, 1993, pp. 87-133.
55. M. Benmouna and B. Hammouda, The zero average contrast condition: Theoretical predictions and experimental examples, *Prog. Polym. Sci.* , 1997, **22**, 49-92.

56. A. I. Nakatani, W. Chen, R. G. Schmidt, G. V. Gordon and C. C. Han, Chain dimensions in polysilicate-filled poly(dimethyl siloxane), *Polymer*, 2001, **42**, 3713-3722.
57. S. Sen, Y. Xie, S. K. Kumar, H. Yang, A. Bansal, D. L. Ho, L. Hall, J. B. Hooper and K. S. Schweizer, Chain conformations and bound-layer correlations in polymer nanocomposites, *Phys. Rev. Lett.* , 2007, **98**, 128302.
58. A. Tuteja, P. M. Duxbury and M. E. Mackay, Polymer Chain Swelling Induced by Dispersed Nanoparticles, *Phys. Rev. Lett.* , 2008, **100**, 077801.
59. K. Nusser, S. Neueder, G. J. Schneider, M. Meyer, W. Pyckhout-Hintzen, L. Willner, A. Radulescu and D. Richter, Conformations of Silica−Poly(ethylene−propylene) Nanocomposites, *Macromolecules*, 2010, **43**, 9837-9847.
60. A.-C. Genix, M. Tatou, A. Imaz, J. Forcada, R. Schweins, I. Grillo and J. Oberdisse, Modeling of Intermediate Structures and Chain Conformation in Silica–Latex Nanocomposites Observed by SANS During Annealing, *Macromolecules*, 2012, **45**, 1663-1675.
61. D. J. Evans, H. J. M. Hanley and S. Hess, Non-Newtonian phenomena in simple fluids, *Phys. Today* 1984, **37**, 26-33.
62. Y. Suzuki, J. Haimovich and T. Egami, Bond-orientational anisotropy in metallic glasses observed by x-ray diffraction, *Phys. Rev. B*, 1987, **35**, 2162-2168.
63. N. J. Wagner and B. J. Ackerson, Analysis of nonequilibrium structures of shearing colloidal suspensions, *J. Chem. Phys.* , 1992, **97**, 1473-1483.
64. G.-R. Huang, Y. Wang, B. Wu, Z. Wang, C. Do, G. S. Smith, W. Bras, L. Porcar, P. Falus and W.-R. Chen, Reconstruction of three-dimensional anisotropic structure from small-angle scattering experiments, *Phys. Rev. E*, 2017, **96**, 022612.
65. Z. Wang, C. N. Lam, W.-R. Chen, W. Wang, J. Liu, Y. Liu, L. Porcar, C. B. Stanley, Z. Zhao, K. Hong and Y. Wang, Fingerprinting Molecular Relaxation in Deformed Polymers, *Physical Review X*, 2017, **7**, 031003.
66. G.-R. Huang, B. Wu, Y. Wang and W.-R. Chen, Characterization of microscopic deformation through two-point spatial correlation functions, *Phys. Rev. E*, 2018, **97**, 012605.
67. C. N. Lam, W.-S. Xu, W.-R. Chen, Z. Wang, C. B. Stanley, J.-M. Y. Carrillo, D. Uhrig, W. Wang, K. Hong, Y. Liu, L. Porcar, C. Do, G. S. Smith, B. G. Sumpter and Y. Wang, Scaling Behavior of Anisotropy Relaxation in Deformed Polymers, *Phys. Rev. Lett.* , 2018, **121**, 117801.
68. R. J. Roe and W. R. Krigbaum, Orientation Distribution Function of Statistical Segments in Deformed Polymer Networks, *J. Appl. Phys.* , 1964, **35**, 2215-2219.
69. M. Kotlarchyk and S. H. Chen, Analysis of small angle neutron scattering spectra from polydisperse interacting colloids, *J. Chem. Phys.* , 1983, **79**, 2461-2469.
70. E. W. Kaler, Small-angle scattering from colloidal dispersions, *J. Appl. Crystallogr.* , 1988, **21**, 729-736.
71. J. S. Pedersen, Analysis of small-angle scattering data from colloids and polymer solutions: modeling and least-squares fitting, *Adv. Colloid Interface Sci.* , 1997, **70**, 171-210.
72. G.-R. Huang, Y. Wang, C. Do, Y. Shinohara, T. Egami, L. Porcar, Y. Liu and W.-R. Chen, Orientational Distribution Function of Aligned Elongated Molecules and Particulates Determined from Their Scattering Signature, *ACS Macro Letters*, 2019, **8**, 1257-1262.
73. A. L. Agapov, V. N. Novikov, T. Hong, F. Fan and A. P. Sokolov, Surprising Temperature Scaling of Viscoelastic Properties in Polymers, *Macromolecules*, 2018, **51**, 4874-4881.

74. G. P. Baeza, C. Dessi, S. Costanzo, D. Zhao, S. Gong, A. Alegria, R. H. Colby, M. Rubinstein, D. Vlassopoulos and S. K. Kumar, Network dynamics in nanofilled polymers, *Nat. Commun.*, 2016, **7**, 11368.
75. Y. Zhou and K. S. Schweizer, Theory for the Elementary Time Scale of Stress Relaxation in Polymer Nanocomposites, *ACS Macro Letters*, 2022, **11**, 199-204.
76. G. Huber and T. A. Vilgis, Universal Properties of Filled Rubbers: Mechanisms for Reinforcement on Different Length Scales, *Kautsch. Gummi Kunstst.*, 1999, **52**, 102-107.
77. A. H. C. o. O. Nomenclature and Symbols, Official symbols and nomenclature of The Society of Rheology, *J. Rheol.* , 2013, **57**, 1047-1055.
78. S. Cheng, Y. Lu, G. Liu and S.-Q. Wang, Finite cohesion due to chain entanglement in polymer melts, *Soft Matter*, 2016, **12**, 3340-3351.
79. G. P. Baeza, A.-C. Genix, C. Degrandcourt, L. Petitjean, J. Gummel, M. Couty and J. Oberdisse, Multiscale Filler Structure in Simplified Industrial Nanocomposite Silica/SBR Systems Studied by SAXS and TEM, *Macromolecules*, 2013, **46**, 317-329.
80. D. Kohls and G. Beaucage, Rational design of reinforced rubber, *Current Opinion in Solid State & Materials Science*, 2002, **6**, 183-194.
81. G. Beaucage, H. K. Kammler and S. E. Pratsinis, Particle size distributions from small-angle scattering using global scattering functions, *J. Appl. Crystallogr.*, 2004, **37**, 523-535.
82. S. Ciccariello, J. Goodisman and H. Brumberger, On the Porod law, *J. Appl. Crystallogr.* , 1988, **21**, 117-128.
83. N. Jouault, F. Dalmas, F. Boué and J. Jestin, Nanoparticles reorganizations in polymer nanocomposites under large deformation, *Polymer*, 2014, **55**, 2523-2534.
84. C. G. Robertson and X. R. Wang, Isoenergetic jamming transition in particle-filled systems, *Phys. Rev. Lett.* , 2005, **95**, 075703.
85. V. F. Sears, Neutron scattering lengths and cross sections, *Neutron News*, 1992, **3**, 26-37.
86. M. K. Crawford, R. J. Smalley, G. Cohen, B. Hogan, B. Wood, S. K. Kumar, Y. B. Melnichenko, L. He, W. Guise and B. Hammouda, Chain Conformation in Polymer Nanocomposites with Uniformly Dispersed Nanoparticles, *Phys. Rev. Lett.* , 2013, **110**, 196001.
87. A. Banc, A.-C. Genix, C. Dupas, M. Sztucki, R. Schweins, M.-S. Appavou and J. Oberdisse, Origin of Small-Angle Scattering from Contrast-Matched Nanoparticles: A Study of Chain and Filler Structure in Polymer Nanocomposites, *Macromolecules*, 2015, **48**, 6596-6605.
88. A.-C. Genix, V. Bocharova, B. Carroll, P. Dieudonné-George, M. Sztucki, R. Schweins, A. P. Sokolov and J. Oberdisse, Direct Structural Evidence for Interfacial Gradients in Asymmetric Polymer Nanocomposite Blends, *ACS Appl. Mater. Interfaces* 2021, **13**, 36262-36274.
89. W.-S. Tung, V. Bird, R. J. Composto, N. Clarke and K. I. Winey, Polymer Chain Conformations in CNT/PS Nanocomposites from Small Angle Neutron Scattering, *Macromolecules*, 2013, **46**, 5345-5354.
90. J. Oderkerk, G. de Schaetzen, B. Goderis, L. Hellemans and G. Groeninckx, Micromechanical Deformation and Recovery Processes of Nylon-6/Rubber Thermoplastic Vulcanizates As Studied by Atomic Force Microscopy and Transmission Electron Microscopy, *Macromolecules*, 2002, **35**, 6623-6629.

91. S. K. Friedlander, K. Ogawa and M. Ullmann, Elastic behavior of nanoparticle chain aggregates: A hypothesis for polymer–filler behavior, *J. Polym. Sci., Part B: Polym. Phys.*, 2000, **38**, 2658-2665.
92. Y. Ikeda, A. Kato, J. Shimanuki, S. Kohjiya, M. Tosaka, S. Poompradub, S. Toki and B. S. Hsiao, Nano-Structural Elucidation in Carbon Black Loaded NR Vulcanizate by 3D-TEM and In Situ WAXD Measurements, *Rubber Chem. Technol.* , 2007, **80**, 251-264.
93. A. Lapra, F. Clément, L. Bokobza and L. Monnerie, Straining Effects in Silica-Filled Elastomers Investigated by Atomic Force Microscopy: From Macroscopic Stretching to Nanoscale Strainfield, *Rubber Chem. Technol.* , 2003, **76**, 60-81.
94. Y. Wang, P. Boukany, S. Q. Wang and X. Wang, Elastic Breakup in Uniaxial Extension of Entangled Polymer Melts, *Phys. Rev. Lett.* , 2007, **99**, 237801.
95. Z.-Y. Wang, D. Kong, L. Yang, H. Ma, F. Su, K. Ito, Y. Liu, X. Wang and Z. Wang, Analysis of Small-Angle Neutron Scattering Spectra from Deformed Polymers with the Spherical Harmonic Expansion Method and a Network Model, *Macromolecules*, 2018, **51**, 9011-9018.
96. I. Popov, B. Carroll, V. Bocharova, A.-C. Genix, S. Cheng, A. Khamzin, A. Kisliuk and A. P. Sokolov, Strong Reduction in Amplitude of the Interfacial Segmental Dynamics in Polymer Nanocomposites, *Macromolecules*, 2020, **53**, 4126-4135.
97. S. Cheng and A. P. Sokolov, Correlation between the temperature evolution of the interfacial region and the growing dynamic cooperativity length scale, *J. Chem. Phys.* , 2020, **152**, 094904.
98. S. Cheng, B. Carroll, W. Lu, F. Fan, J.-M. Y. Carrillo, H. Martin, A. P. Holt, N.-G. Kang, V. Bocharova, J. W. Mays, B. G. Sumpter, M. Dadmun and A. P. Sokolov, Interfacial Properties of Polymer Nanocomposites: Role of Chain Rigidity and Dynamic Heterogeneity Length Scale, *Macromolecules*, 2017, **50**, 2397-2406.
99. S. Cheng, B. Carroll, V. Bocharova, J.-M. Carrillo, B. G. Sumpter and A. P. Sokolov, Focus: Structure and dynamics of the interfacial layer in polymer nanocomposites with attractive interactions, *J. Chem. Phys.* , 2017, **146**, 203201.
100. B. Carroll, S. Cheng and A. P. Sokolov, Analyzing the Interfacial Layer Properties in Polymer Nanocomposites by Broadband Dielectric Spectroscopy, *Macromolecules*, 2017, **50**, 6149-6163.
101. S. Cheng, Broadband Dielectric Spectroscopy of Polymer Nanocomposites, in *Broadband Dielectric Spectroscopy: A Modern Analytical Technique*, American Chemical Society, 2021, vol. 1375, ch. 7, pp. 157-183.
102. C. Fernández-de-Alba, A. M. Jimenez, M. Abbasi, S. K. Kumar, K. Saalwächter and G. P. Baeza, On the Immobilized Polymer Fraction in Attractive Nanocomposites: Tg Gradient versus Interfacial Layer, *Macromolecules*, 2021, **54**, 10289-10299.
103. M. Kawaguchi, K. Hayakawa and A. Takahashi, Adsorption of Polystyrene onto Silica at the Theta Temperature, *Polym. J.* , 1980, **12**, 265-270.
104. R. D. Priestley, L. J. Broadbelt, J. M. Torkelson and K. Fukao, Glass transition and alpha-relaxation dynamics of thin films of labeled polystyrene, *Phys. Rev. E*, 2007, **75**, 061806.
105. B. A. Pazmino Betancourt, J. F. Douglas and F. W. Starr, Fragility and cooperative motion in a glass-forming polymer-nanoparticle composite, *Soft Matter*, 2013, **9**, 241-254.
106. E. J. Bailey and K. I. Winey, Dynamics of Polymer Segments, Polymer Chains, and Nanoparticles in Polymer Nanocomposite Melts: A Review, *Prog. Polym. Sci.* , 2020, 101242.

107. K. S. Schweizer and D. S. Simmons, Progress towards a phenomenological picture and theoretical understanding of glassy dynamics and vitrification near interfaces and under nanoconfinement, *J. Chem. Phys.* , 2019, **151**, 240901.
108. J. Song, R. Kahraman, D. W. Collinson, W. Xia, L. C. Brinson and S. Keten, Temperature effects on the nanoindentation characterization of stiffness gradients in confined polymers, *Soft Matter*, 2019, **15**, 359-370.
109. D. W. Collinson, R. J. Sheridan, M. J. Palmeri and L. C. Brinson, Best practices and recommendations for accurate nanomechanical characterization of heterogeneous polymer systems with atomic force microscopy, *Prog. Polym. Sci.* , 2021, **119**, 101420.
110. B. D. Vogt, Mechanical and viscoelastic properties of confined amorphous polymers, *J. Polym. Sci., Part B: Polym. Phys.*, 2018, **56**, 9-30.